Charles University in Prague
Faculty of Mathematics and Physics

MASTER THESIS

Marek Scholz

Methods of Study of Photosensitizer-Photophysics with Application on Thiazolyl-porphyrins

Department of Chemical Physics and Optics

Supervisor of the master thesis:	RNDr. Roman Dědic, Ph.D.
Study programme:	Physics
Specialization:	Biophysics and Chemical Physics

Prague 2011

I want to express my appreciation to my supervisor RNDr. Roman Dědic, Ph.D. for his valuable advice and tutoring. Great thanks belong to Dr. Santi Nonell and to the whole group of photophysics at Institut Químic de Sarrià, Universitat Ramon Llull, Barcelona, for their constant and kind help during my research stay in Barcelona. Special thanks belong to Ruben Ruiz, Clara Zazo, Fernando Aliste and Leticia Fernandéz – they all know why. Finally, I'd like to thank my family heartily for their perpetual support under all conditions.

I declare that I carried out this master thesis independently, and only with the cited sources, literature and other professional sources.

I understand that my work relates to the rights and obligations under the Act No. 121/2000 Coll., the Copyright Act, as amended, in particular the fact that the Charles University in Prague has the right to conclude a license agreement on the use of this work as a school work pursuant to Section 60 paragraph 1 of the Copyright Act.

In ..... date ..... Signature

Contents

1 Preface **6**

2 Introduction **7**
2.1 Basic Concepts . . . 7
2.2 Photosensitizers . . . 9
2.3 Photosensitizers for Photodynamic Therapy . . . 10
2.4 Standards for $^1O_2$ Quantum Yield Measurements . . . 12
2.5 Sulphur Effect . . . 13

3 Experimental methods and data handling **15**
3.1 Absorption Spectra . . . 15
3.2 Fluorescence Steady State Spectra . . . 15
3.3 Fluorescence Lifetime . . . 15
3.4 Flash-photolysis: Triplet Lifetimes and T-S Spectra . . . 17
3.5 Singlet Oxygen Phosphorescence . . . 18
3.6 Delayed Fluorescence . . . 19
3.7 Photosensitizer Phosphorescence Spectrum . . . 21
3.8 Laser-induced Optoacoustic Spectroscopy . . . 22
3.8.1 Separation of Structural and Thermal Volume Changes . . . 22
3.8.2 Experimental Setup . . . 24
3.8.3 Quantum Yields of Singlet Oxygen and PS Triplet . . . 25
3.8.4 Obstacles . . . 26
3.9 Microscopy . . . 28

4 Results and discussion **31**
4.1 Solubility . . . 31
4.2 Absorption Spectra . . . 31
4.3 Fluorescence . . . 33
4.4 Triplet Lifetimes and T-S Absorption . . . 33
4.5 Singlet Oxygen Production . . . 36
4.6 Quantum Yields by Optoacoustic Spectroscopy . . . 36
4.7 Delayed Fluorescence . . . 41
4.8 Photosensitizer Phosphorescence . . . 41
4.9 Microscopy . . . 46

5 Conclusions **48**

Table of results **49**

References **50**

List of Abbreviations **54**

Attachment: Octave code **56**

Název práce: Metody výzkumu fotofyziky fotosensibilizátorů s aplikací na thiazolyl-porfyriny
Autor: Marek Scholz
Katedra: Katedra chemické fyziky a optiky
Vedoucí diplomové práce: RNDr. Roman Dědic, Ph.D.
e-mail vedoucího: Roman.Dedic@mff.cuni.cz

Abstrakt: Fotodynamická terapie onkologických a dalších závažných onemocnění je prudce se rozvíjející léčebnou metodou. Principem jejího účinku je generace vysoce reaktivního singletního kyslíku a volných radikálů přenosem excitační energie z molekul tzv. fotosensibilizátorů, které se selektivně usazují v postižené tkáni a při léčbě jsou excitovány lokálním ozářením příslušné tkáně. Vzniklé reaktivní formy molekul potom způsobí apoptózu nebo nekrózu postižených buněk a tím i likvidaci postižené tkáně. Zásadním článkem ve vývoji fotodynamických metod je příprava účinných a biologicky kompatibilních fotosensibilizačních barviv spolu s jejich následnou podrobnou fotofyzikální charakterizací. Práce se zaměřuje na vysvětlení nejpoužívanějších metod výzkumu fotofyziky fotosensibilizátorů a jejich aplikaci na nově syntetizovaná fotosensibilizační barviva: thiazolyl-porfyriny. Byly použity metody absorpční a fluorescenční spektroskopie, časově a spektrálně rozlišená detekce luminescence, flash-fotolýza, optoakustická spektroskopie a další. Thiazolyl-porfyriny se ukázaly být perspektivními fotosensibilizátory s kvantovým výtěžkem singletního kyslíku blízko jedničce. Součástí práce byl rovněž vývoj aparatury pro mikroskopické zobrazování infračervené luminescence s využitím unikátní zesilované infračervené kamery. Tato metoda má potenciál významně přispět k pochopení účinku fotosensibilizátorů přímo v živých buňkách. Práce byla vypracována ve spolupráci s Institut Químic de Sarrià, Universitat Ramon Llull, Barcelona.
Klíčová slova: thiazolyl-porfyrin, fotosensibilizátor, singletní kyslík, fosforescence, kvantový výtěžek

Title: Methods of Study of Photosensitizer-Photophysics with Application on Thiazolyl-porphyrins

Author: Marek Scholz
Department: Department of Chemical Physics and Optics
Supervisor: RNDr. Roman Dědic, Ph.D.
Supervisor's e-mail address: Roman.Dedic@mff.cuni.cz

Abstract: Photodynamic therapy for oncologic and various chronic diseases is a rapidly emerging method of treatment. It is based on the production of highly reactive singlet oxygen and free radicals by excitation energy transfer from the molecules of photosensitizers. Photosensitizers are preferentially accumulated in the target tissues and locally illuminated. This way produced reactive species cause apoptosis or necrosis of the cells leading to the desired therapeutic effect. Synthesis and subsequent photophysical characterization of photosensitizing dyes is a fundamental part of the development of photodynamic methods. The main aim of the work is to explain the most widely used methods of photophysical study of photosensitizers and apply them to new synthesized photosensitizers: thiazolyl-porphyrins. Methods of absorption and fluorescence spectroscopy, flash-photolysis, time- and spectral-resolved detection of luminescence, optoacoustic spectroscopy and other spectroscopic methods were used. Thiazolyl-porphyrins proved to be promising new photosensitizers with singlet oxygen quantum yield close to unity. The work also contains the development of an experimental setup for microscopic imaging of infrared luminescence using a unique intensified infrared camera. This method could significantly contribute to the understanding of the effects of photosensitizers directly in living cells. The work was done in collaboration with Institut Químic de Sarrià, Universitat Ramon Llull, Barcelona.
Keywords: thiazolyl-porphyrin, photosensitizer, singlet oxygen, phosphorescence, quantum yield

1 Preface

Singlet oxygen, the lowest excited state of molecular oxygen, is a fascinating species in many ways. Its chemistry differs significantly from that of ground state triplet oxygen. Singlet oxygen readily reacts with a wide range of biological and organic materials which leads to their alteration and degradation. Arguably the most important way of singlet oxygen formation is the so-called photosensitizing process: A light excited molecule of an appropriate dye transfers energy to molecular oxygen giving rise to singlet oxygen. Nature is figuratively full of such dyes which support the formation of singlet oxygen, e.g. photosynthetic dyes or Protoporphyrin IX (a precursor for heme). Singlet oxygen is involved in a rich variety of diverse biochemical processes, such as photosynthesis, cell signaling, immune responses or polymer degradation [27]. Research involving singlet oxygen and the photosensitizing process has various perspectives [39]. Photodynamic therapy for cancer and other diseases is an especially interesting research field – it's a promising medical treatment with potential to be widely used. Therefore, preparation, characterization and clinical research of novel highly effective photosensitizing drugs is an important task for the present and future science.

This work focuses on the photophysical characterization of two newly synthesized photosensitizers – Thiazolyl-porphyrins (figure 2.4). New compounds are compared to the chemically related and well known tetraphenylporphin (TPP) shown in figure 2.5. The presence of sulphur atoms is supposed to enhance intersystem crossing leading to improved triplet and singlet oxygen quantum yields. Thiazolyl-porphyrins are investigated as potential photosensitizing standards and reference compounds with high quantum yields of singlet oxygen. The relation between photophysical properties and chemical structure is discussed. The compounds were examined mostly in three solvents – toluene, tetrahydrofuran (THF) and dimethylformamid (DMF). The most important photophysical properties obtained are summarized in the table at the end of the text.

An improvement and optimization of experimental and data-handling protocol for optoacoustic spectroscopy measurements of quantum yields were done and are presented. Part of the work focuses on the development of an experimental setup for microscopic imaging of infrared luminescence using a unique intensified infrared camera. This novel method could significantly contribute to the understanding of the photosensitizing process directly in living cells. Besides experimental results, the work intends to provide a brief description and explanation of several general photophysical techniques used for investigation of photosensitizer photophysics.

2 Introduction

2.1 Basic Concepts

The ground state of the majority of molecules is of a singlet spin-configuration, whereas the lowest excited state is of a triplet spin-configuration. Two electrons residing in one orbital have an antisymmetric spin-part of wavefunction (singlet configuration) according to the Pauli principle. If one of the paired electrons is excited to a higher orbital, a wavefunction with symmetric spin-part (triplet) and antisymmetric space-part is energetically favourable. The antisymmetric space-part resulting in zero probability of encountering the electrons at the same spot better reflects a repulsive electric force between electrons [18].

In contrast, the ground state of an oxygen molecule is biradical due to high symmetry leading to high degeneracy. There are two unpaired electrons with parallel spin resulting in a triplet spin-configuration of the ground state. The lowest lying excited state has paired electrons with a singlet spin-configuration and is called singlet oxygen ($^1\Delta_g$ electronic configuration). A scheme of electronic orbitals for triplet and singlet oxygen is shown in figure 2.1. Singlet oxygen exerts weak phosphorescence around 1275nm (transition to ground state is spin-forbidden)[42]. The reactivity of singlet oxygen is significantly higher than that of ground state oxygen because its spin-multiplicity matches the multiplicity of the ground state of a majority of molecules.

Singlet oxygen is an effective oxidant and typically attacks carbon double bonds of organic compounds. Singlet oxygen is able to attack lipids, amino-acids, proteins or nucleic acids and its higher production can even induce cell death [12, 16].

One of the most important ways of singlet oxygen production is photosensitizing process: Energy transfer from the excited triplet state of the so-called photosensitizer (PS) molecule to ground state triplet oxygen gives rise to singlet oxygen. Triplets of PS are created by intersystem-crossing from light-excited singlet states. The whole photosensitizing process is illustrated in figure 2.2. Triplets of PS also exhibit weak phosphorescence as the transition to the singlet ground state is spin-forbidden.

The quantum yield of singlet oxygen production Φ_Δ is a very important characteristic of a PS. It's defined as the ratio of the number of singlet oxygen molecules originated to the number of photons absorbed by PS. Analogically, the quantum yield of PS triplet production Φ_T is defined as the ratio of the number of PS triplets originated to the number of photons absorbed by PS. PS singlet, PS triplet, or singlet oxygen decay by various pathways. Corresponding rate constants are defined for each decay pathway. The rate constant for a given decay process of an excited state can be calculated as the ratio Φ/τ where Φ is the fraction of excited states decaying by a given process and τ is the lifetime of the excited state [35].

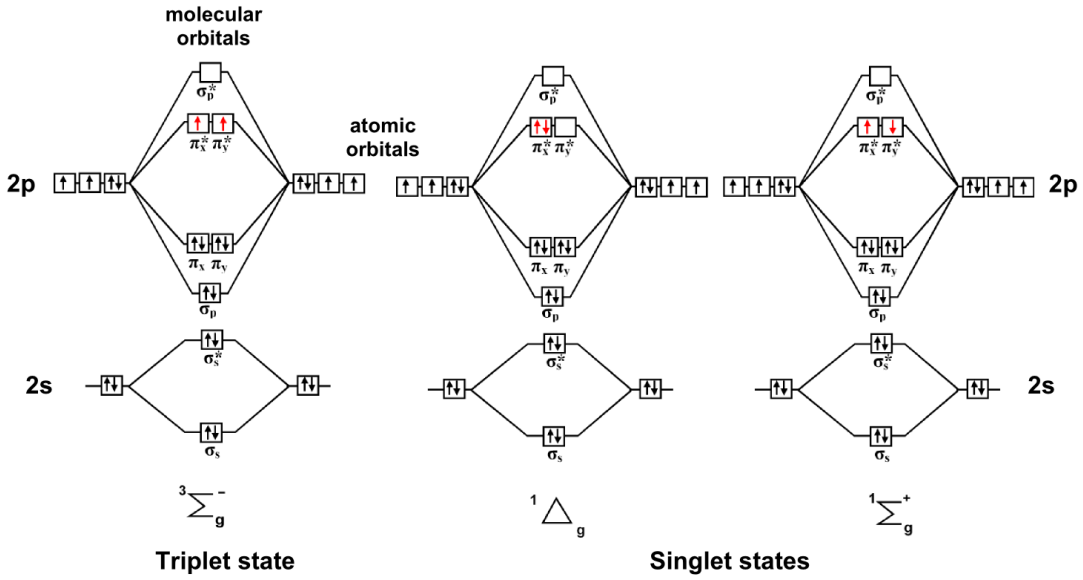

Figure 2.1: Molecular orbitals of ground triplet oxygen and the excited singlet oxygen molecule. Adapted from [49].

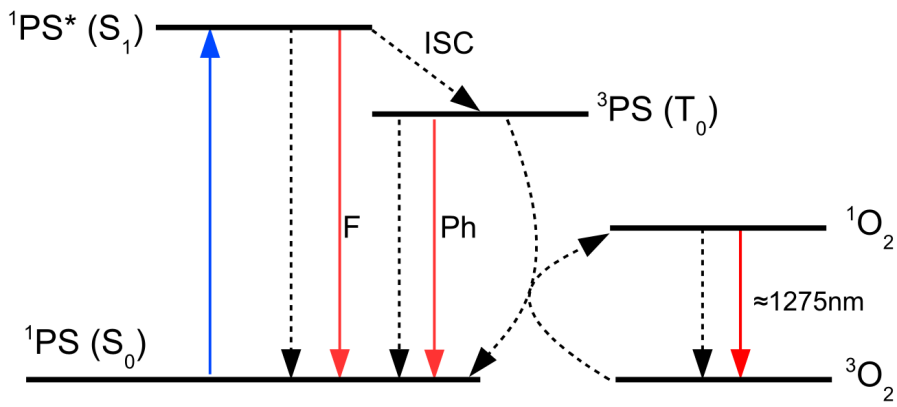

Figure 2.2: Schematic view of the photosensitizing process. Coloured arrows stand for radiative transitions, black ones for non-radiative. F denotes fluorescence, Ph phosphorescence, and ISC intersystem-crossing. Vibrational structure is not shown for the sake of simplicity.

2.2 Photosensitizers

Photosensitizer dye is usually a molecule able to absorb a photon and transit from an excited singlet state to a triplet state by intersystem-crossing. There are two major pathways for PS triplet action referred to as type I and type II processes. The type I process leads to the generation of highly reactive free radicals (superoxide anion, hydroxyl radical ...) via electron or hydrogen transfer from the PS triplet to substrate. The type II reaction involves energy transfer from the photosensitizer triplet to oxygen molecule giving rise to singlet oxygen. (Electron transfer from PS triplet to oxygen yielding superoxide anion is sometimes called type II reaction as well [39]). The energy of the PS triplet needs to be suitably higher than the energy of singlet oxygen in order to provide efficient photosensitization. Both the type I and type II processes ultimately cause oxidative degradation of biomolecules.

Photosensitizers are mostly chromophores with a system of conjugated double bonds. Porphyrin-based PS form a great and very important group of PS and are of special interest with respect to this work. Many naturally occurring compounds are of porphyrin nature, for example chlorophylls or heme. Extensive description of photophysics of porphyrins is provided at [1]. The structure of the porphyrin core is shown in figure 2.3. The system of conjugated double bonds with 18 π-electrons is responsible for characteristic UV-Vis absorption spectra. There is one very strong absorption band (Soret band) around 400 nm corresponding to the $S_0 \rightarrow S_2$ transition. Three weaker absorption bands (Q-bands) are present approximately between 500 nm and 600 nm corresponding to the $S_0 \rightarrow S_1$ transition. Many various modifications of porphyrin-based PS were reported and described. The central cavity in the porphyrin core allows for the coordination of a metal atom. Meso- and β- carbons of the porphyrin core are the most reactive sites and the hydrogen can be substituted. Also, the pyrolle peripheral double bond can be reduced (e.g. chlorins). A short list of various porphyrin-based photosensitizers follows.

Porphyrins. Hematoporphyrin (HP) or Protoporphyrin IX (PPIX) naturally occur in mammalian blood and can be readily isolated. A variety of their derivatives have been described and their photosensitizing effect reported. PPIX, an excellent photosensitizer, is naturally synthesized from aminolevulinic acid (ALA) and consequently converted to heme [33]. Important members of porphyrins are meso-substituted porphyrins, tetra-phenyl-porphin (TPP) or ionic water soluble tetra-pyridyl-porphin (TMPyP), which are readily synthesized and metalated and provide a wide range of derivatives with photodynamic effect. Tetra-sulphonated-phenyl-porphyrin ($TPPS_4$) is another water soluble ionic photosensitizer widely used in laboratories as a reference PS. Great amounts of various PS can be prepared by substitutions at meso- or β- carbon and by chelating with metal ions providing PS with very different biological properties and functions [1].

Metalloporphyrins. Metal atoms such as Mg, Fe, Zn, Pd, Pt and others can be coordinated in the central cavity of porphyrin-based compounds (e.g. chlorophyll or heme). Coordination of the metal atom leads to higher symmetry due to the loss of hydrogen atoms resulting in significant alteration of Q-bands structure (a reduced number of Q-bands). The metal atom can sometimes enhance spin-orbit coupling due to heavy atom effect leading to enhanced intersystem-crossing [4].

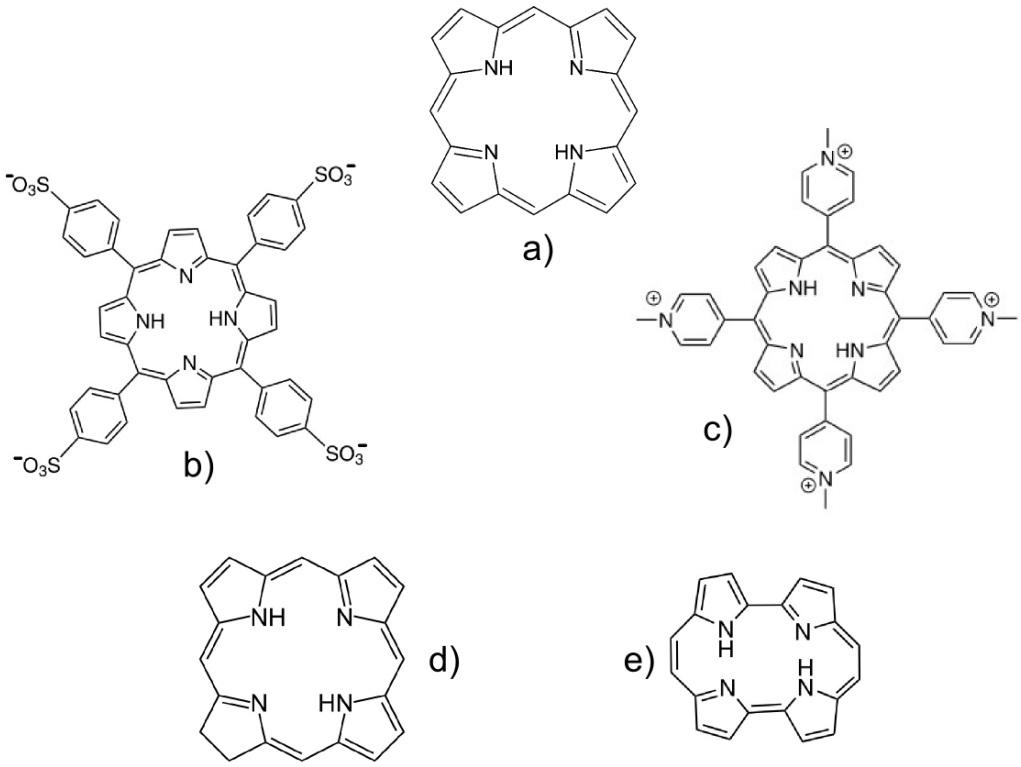

Figure 2.3: (a) Porphin core, (b) $TPPS_4$, (c) TMPyP, (d) Chlorin core, (e) Porphycene core

Chlorins are distinguished by the loss of one peripheral pyrolle double bond with respect to porphyrin (figure 2.3). A strong absorption band at the red portion of the spectrum ($650 - 680\,\mathrm{nm}$) appears due to the loss of symmetry [12, 45]. This feature is important with respect to application in photodynamic therapy (section 2.3). Chlorophylls also lack one peripheral double bond and are extensively used for the preparation of various chlorins.

Porphycenes. Porphycene is a structural isomer of porphyrin. Unsubstituted porphycene is shown in figure 2.3. There is a modification in core-structure and less symmetry compared to the porphyrin-core. Porphycenes are more photostable than porphyrins. The loss of symmetry leads to approximately ten-fold stronger absorption at Q-bands and five-fold weaker absorption at the Soret band [10]. Porphycenes are strongly fluorescent. These features are favourable for clinical applications (photodynamic therapy, fluorescence imaging). Despite the fact that the central cavity is deformed, porphycenes are able to make stable complexes with a variety of metal cations [1].

2.3 Photosensitizers for Photodynamic Therapy

Photodynamic therapy is a very important and promising application of photosensitizers in medicine. Singlet oxygen and free radicals produced via the photosensitizing process can be used for fighting cancer, other lesions (e.g. macular degeneration), or even bacteria and viruses [2, 3, 17]. The photosensitizer is administrated to the patient and is more or less selectively absorbed by cells of

the targeted tissue. The particular spot is then irradiated by visible light and singlet oxygen and other reactive species are produced at the spot. Oxidative stress can induce apoptosis or necrosis of cells of the targeted tissue. The selectivity of photodynamic therapy is reached both by the selective absorption of the photosensitizer and by localized irradiation. A nice summary of PDT research is provided at [12–14]

Searching for an appropriate photosensitizer is a crucial part of research in the field of photodynamic therapy. Different types of photosensitizers will probably be needed for different applications. Nevertheless, some of the general requirements which a good photosensitizer should fulfill are listed below.

Absorption bands should lay at wavelengths of therapeutic window 600 nm – 1000 nm where the depth of penetration into human tissue is maximal. Absorption coefficients should be in the range of $10^4\,\mathrm{M}^{-1}\mathrm{cm}^{-1}$. Absorption coefficients which are too high are undesirable due to the self-shielding effect [20]. On the other hand, strong absorption at shorter wavelengths is unfavorable because of potential skin photosensitivity to sun-light. As mentioned before, porphyrins show strong Soret band around 400 nm and Q-bands between 500 nm and 600 nm, which is not ideal with respect to the presented aspects. Chlorins, phtalocyanines or porphycenes show enhanced and red-shifted Q-bands together with relatively weaker Soret band compared to porphyrins and thus are more convenient. Absorption bands at wavelengths over 800 nm mean that PS triplet energy probably won't be sufficient to enable energy transfer to oxygen [12].

The main cytotoxic agent is considered to be singlet oxygen, but so far it hasn't been proved *in vivo* conditions, where binding of a photosensitizer to cellular macromolecules could favor a type I photodynamic pathway [1]. High quantum yield of triplet production is required and most photosensitizers currently under evaluation also exert high singlet oxygen quantum yield. On the other hand, quantum yields close to one are not necessary. Lower quantum yields can be counterbalanced by other profitable features such as selectivity to cancer, convenient sub-cellular localization and others. Fluorescence is a process competing with intersystem-crossing, but most photosensitizers for PDT are fluorescent and it is considered a favourable feature. Fluorescence allows for imaging of PS localization, which can serve for diagnostic purposes and visualization of targeted tissue. Fluorescence can be used to quantify the amount of PS accumulated in tissue allowing to set an appropriate light dose. A control over photobleaching of PS is also possible [12].

It has been known for a long time that naturally occurring hematoporphyrin is preferentially accumulated in tumor tissue [1, 22]. This is generally one of the most important features of tetrapyrolle photosensitizers with respect to PDT. Various mechanisms leading to preferential accumulation of tetrapyrolles in a tumor have been suggested and investigated. A few of them are picked up and described in order to illustrate the situation. PS may aggregate with serum proteins after administration. Serum protein works as a carrier and penetrates into tumor cells. One theory claims that the binding of PS to low-density-lipoprotein (LDL) is of major importance. Tumor cells have over-expressed LDL receptors. It leads to extensive penetration of LDL into tumor cells allowing them to gain cholesterol needed for the biosynthesis of lipids and rapid growth [34]. Another theory claims that PS aggregates or porphyrin-lipoprotein complexes

are phagocyted by macrophages which infiltrate solid tumors to a wider extent [31]. Photosensitizers which show fast pharmacokinetics (the best performance is reached within a few hours after administration) are believed to bind to albumin which readily penetrates into tumor cell due to increased vascular permeability typical for tumor cells [51]. The ability to bind to proteins and to self-aggregate is mainly influenced by the hydrophilic or hydrophobic nature of PS which is dependent on the nature of substituents on the tetrapyrolle ring. Selectivity can be improved by conjugating tetrapyrolle-based PS with suitable side-groups or even whole carrier vehicle which is readily uptaken by tumor cells. For example, folic-acid receptors are overexpressed in various tumor cells and attempts to target PS through conjugation with folic acid have been made [23, 37]. Recently, very promising experiments have been made with delivery-vehicles based on silica nanoparticles. Nanoparticles can be designed to have a good rate of permeability into tumor cells and to support active targeting via ligands recognizing tumor-associated markers. Moreover, the porous structure allows for excellent retention of hydrophobic PS and oxygen penetration into the nanoparticle [7, 15, 52].

The tumor destruction is considered to be driven by three main mechanisms: Direct cell death by apoptosis, necrosis, or autophagocytosis [11], destruction of tumor vasculature, and activation of immune response against tumor cells (due to inflammatory signaling from damaged tissue after PDT).

There are several more requirements imposed on a good clinical photosensitizer. PS should show low dark-toxicity, rapid elimination from the body, a stable and well defined chemical structure, and easy synthesis from well available materials. Time interval between PS administration and light delivery is a crucial parameter of PDT treatment [14]. The damage made by $^1O_2$ is strongly dependent on the sub-cellular localization of PS making this feature also very important. For example mitochondria has been found to be a very efficient target for PS used in PDT [12].

2.4 Standards for $^1O_2$ Quantum Yield Measurements

Many experimental techniques for the measurement of singlet oxygen quantum yields (Φ_Δ) rely on comparison with standards of known quantum yields. Among such techniques belong direct $^1O_2$ luminescence measurements or methods based on chemical probes which change fluorescence or absorption spectra after a reaction with $^1O_2$. It's complicated to determine Φ_Δ precisely, even for standards (see sections 4.5 and 4.6). There is a variety of commonly used standards, both polar and non-polar and with different absorption spectra. A suitable standard has to be chosen especially with respect to the solvent and excitation wavelength.

Reviews [40] and [50] provide a nice summary of Φ_Δ of various compounds. Phenalenone is a very useful standard with Φ_Δ close to unity for a wide range of solvents [41]. Fullerene C_{60} has Φ_Δ close to unity both in benzene and toluene. TPP is a very common standard with Φ_Δ around 0.7 in a wide range of non-polar solvents. TPPS, $TPPS_4$ or $TMPyPH_2$ are water soluble standards with Φ_Δ around 0.7 as well. Acridine, anthracene, methylene blue or rose bengal, all polycyclic organic compounds, are frequently used as well.

2.5 Sulphur Effect

Two newly synthesized photosensitizing dyes, MonoThiazolyl- and BiThiazolyl-porphin, are shown in figure 2.4. The structures are compared to related TPP (figure 2.5). Detailed spectroscopic characterization of these compounds is the main goal of this work. The introduction of four relatively heavier atoms – sulphurs – close to the chromophore of the porphyrin may result in an enhanced intersystem-crossing. Should that be the case, an enhancement of singlet oxygen quantum yield (Φ_Δ) should be observed as well since singlet oxygen is produced by energy transfer from the triplet state. Several works regarding effect of sulphur atoms on enhancement of intersystem-crossing have been published before. In the case of sulphur substituted squaraines the enhancement was interpreted according to the El-Sayed rule as a result of an inversion of the lowest π-π^* transition by an n-π^* transition [48]. In the case of core-substituted porphyrin the enhancement was explained by the effects of heavier nucleus (enhanced spin-orbit coupling) and coupling of empty d-orbitals of sulphur with the π-system of porphyrin [29]. On the other hand, a selenium substituted core shows a decrease in triplet quantum yield [28]. The term 'heavy atom' usually refers to atoms remarkably heavier than sulphur, such as bromine, iodine or platinum. Metals (e.g. platinum) coordinated in the porphyrin core may enhance the transition between singlet and triplet sometimes leading to relatively stronger phosphorescence emission [6]. Bromine or iodine substituted porphyrins also may show enhanced triplet yields. The heavy atom effect seems to be more pronounced when heavy atoms are closer to the system of conjugated double bonds [28].

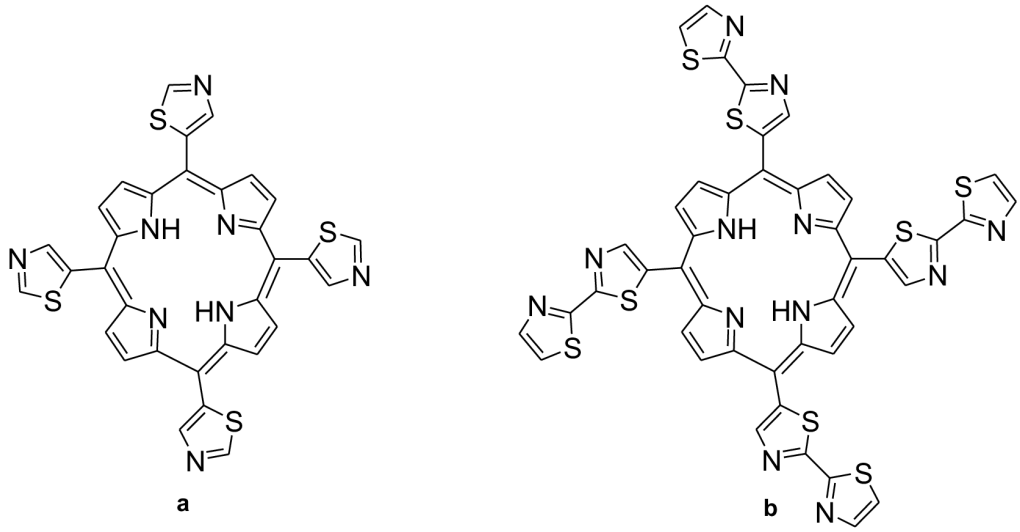

Figure 2.4: a) MonoThiazolyl-porphin, b) BiThiazolyl-porphin

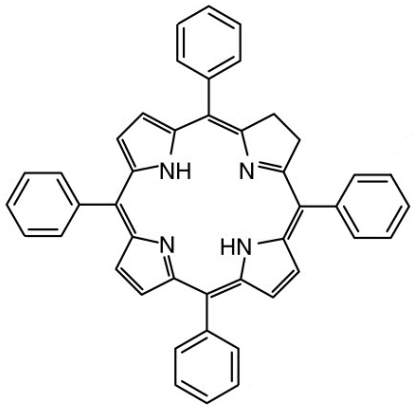

Figure 2.5: Tetraphenylporphin (TPP)

3 Experimental methods and data handling

3.1 Absorption Spectra

Absorption spectra were recorded on a Varian Cary 4E spectrophotometer. A dependence of sample absorbance A on concentration c was measured. The slope of linear fit provides the extinction coefficient ε ($A = \varepsilon cl$). Absorbance measurements are reliable up to a value of 2, higher absorbances are very noisy. Precise absorbance matching of several samples is a crucial step in quantum yield measurements. All the samples to be compared need to absorb the same amount of photons. Energy absorbed by the sample is proportional to the term $1 - 10^{-A}$ according to the Lambert-Beer law. This term can be used as a correction factor if there is some absorbance mismatch among samples. Mostly, samples of absorbances of about 0.1 were prepared. It corresponds to concentrations around $10 - 20\,\mu\mathrm{M}$ in the case of 532 nm excitation. Absorbances were routinely checked before and after those experiments which were prone to photobleaching.

3.2 Fluorescence Steady State Spectra

Fluorescence excitation and emission spectra were recorded on a Jobin Yvon-Spex Fluoromax-2 spectrofluorometer. Fluorescence quantum yields (Φ_F) were determined by the comparison of areas under emission curves for absorbance-matched solutions of both the samples and a standard. Meso-5,10,15,20-tetraphenyl porphin (TPP) in toluene was used as a standard with $\Phi_\mathrm{F} = 0.11$ [43]. The samples were excited at 532 nm, and absorbances of the samples were matched at excitation wavelength and kept below 0.05 in the fluorescence region in order to prevent inner-filter effects. The quantum yield is calculated

$$\Phi = \Phi_\mathrm{R} \frac{I n^2}{I_\mathrm{R} n_\mathrm{R}^2}\,, \tag{3.1}$$

where I is the area under the emission curve and n is the refractivity index of solvent (R denotes reference sample)[35, chapter 2].

3.3 Fluorescence Lifetime

Lifetimes of fluorescence (τ_S) of the investigated compounds are in nanosecond-range, but fluorescence lifetimes can be commonly substantially shorter than one nanosecond. Therefore, time-resolution in picosecond scale is required for lifetime and kinetic measurements. For this purpose the Time-Correlated Single Photon Counting (TCSPC) method is used [8]. Fluorescence lifetime corresponds to the lifetime of the first excited singlet state and together with the value of fluorescence

quantum yield can be used to compute radiative and non-radiative decay rate constants.

Experimental setup and data handling. The sample was excited by a focused picosecond pulsed diode laser (375 nm) working at a 10 MHz repetition rate. The signal passes through a monochromator into PicoQuant Fluotime 200 time-correlated single photon counting system equipped with a red-sensitive photomultiplier. A detailed description of TCSPC technique can be found in [8] and a short summary is provided here. TCSPC technique consists in measuring the time elapsed between the laser pulse and the first photon detected. Values of times measured are put in histogram forming fluorescence kinetics. Short fluorescence lifetimes enable high laser pulse repetition rates. Light intensity has to be so low that the probability of detecting one photon in one period between laser pulses is far less than 1. Excitation laser pulse triggers a time-to-amplitude converter (TAC). The first detected photon stops the amplitude build-up and TAC returns an output signal proportional to the time elapsed between the start and stop pulse. The signal from TAC is fed into an analog-to-digital converter providing the digital equivalent of the photon detection time, which addresses a corresponding data-memory location and adds '1' in there. Gradually, the histogram of photon detection times is built-up in the data-memory. It's necessary to ensure that a photon is detected in no more than 1% of signal periods in order to diminish the number of periods where more than one photon comes. In each period only the first photon is detected and the latter ones are ignored. Higher light intensities would lead to distortion of the histogram. Amplified single-photon-induced pulses from a photomultiplier (PMT) have more or less random amplitude and low amplitude noise-pulses are present. Therefore, signal enters a discriminator, a device with an adjustable threshold which differentiates photon-pulses from noise pulses delivering pulses of constant duration and defined logical value. As time-resolution is critical for TCSPC measurements, the discriminator which triggers at a constant fraction of the pulse amplitude is employed in order to suppress timing errors due to the amplitude jitter of incoming PMT pulses. This feature leads to efficient background- and gain-noise suppression. Time-resolution is limited mainly by transit-time spread. Time-resolution can be much better than time-width of single photon response of the system or time-width of the excitation pulse (the measured curve can be deconvoluted)[8].

The measured signal is the result of a convolution of a laser pulse time-shape with actual fluorescence decay curve. The time-shape of the laser pulse is obtained from a scattering sample by measuring near to the laser-wavelength. Measured signal is then fitted by convolution of the laser pulse time-shape with exponential decay. If more than one exponential (biexponential or even triexponential) is needed to fit the signal, then more than one form of fluorophore is present (various forms of investigated compound or some kind of impurities).

The radiative decay rate constant of the first excited singlet state is calculated as $k_{\mathrm{R}} = \Phi_{\mathrm{F}}/\tau_{\mathrm{S}}$, where τ_{S} is the first excited singlet state lifetime (corresponding to fluorescence lifetime) Analogically, the non-radiative decay rate constant equals $k_{\mathrm{NR}} = (1 - \Phi_{\mathrm{F}})/\tau_{\mathrm{S}}$.

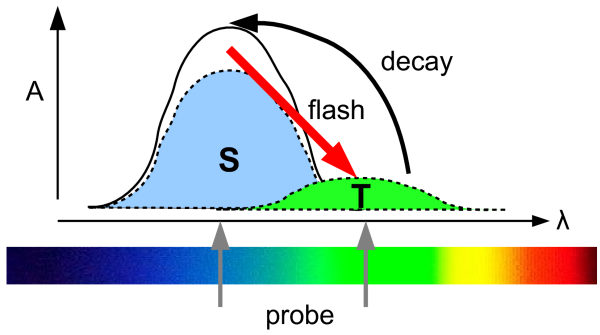

Figure 3.1: Schematic view of T-S spectra principle.

3.4 Flash-photolysis: Triplet Lifetimes and T-S Spectra

Flash-photolysis belongs among pump-probe techniques. The technique allows to observe triplet state kinetics of photosensitizers. A laser pulse brings some of the ground state PS molecules into excited singlet states. Some of the excited singlet states consequently undergo intersystem-crossing giving rise to triplet states. The ground state was depopulated and excited triplet states were populated. Excited triplet states can absorb into higher triplet states. Different absorption spectra and extinction coefficients correspond to the ground state and excited triplet state. The excited triplet state gradually depletes leading to recovery of the ground state population. The situation is illustrated at picture 3.1. A time-resolved absorption measurement of the sample after the excitation pulse can follow the change of absorption spectrum providing the decay curve of the excited triplet state and its lifetime.

The measured quantity is usually the difference between the absorbance of the sample at time t after excitation and absorbance before excitation

$$\begin{aligned} \Delta A(t,\lambda) &= \varepsilon_{\mathrm{S}}(\lambda)[S_0](0) - (\varepsilon_{\mathrm{S}}(\lambda)\,([S_0](0) - [T_1](t)) + \varepsilon_{\mathrm{T}}[T_1](t)) \\ &= (\varepsilon_{\mathrm{T}}(\lambda) - \varepsilon_{\mathrm{S}}(\lambda))\,[T_1](t)\,, \end{aligned} \tag{3.2}$$

where $[S_0](0)$ is the concentration of ground states before excitation, $[T_1](t)$ concentration of excited triplet states at time t after excitation, and ε_{S}, ε_{T} are corresponding extinction coefficients. The resulting $\varepsilon_{\mathrm{T-S}}(\lambda) = \varepsilon_{\mathrm{T}}(\lambda) - \varepsilon_{\mathrm{S}}(\lambda)$ is the so called triplet minus singlet (T-S) absorption spectrum. The fit of $\Delta A(t)$ kinetics readily provides the lifetime of triplets.

A Q-switched Nd:YAG laser (Surelite I-10, Continuum) with right-angle geometry at wavelength of 532 nm with pulse width $\sim$ 5 ns was used to populate triplets, a Xe lamp (PTI, 75 W) was used as a probe. The signal passes through a dual-grating monochromator (mod. 101, PTI) coupled to a photomultiplier (Hamamatsu R928) and afterwards is fed to an oscilloscope, where the time-resolved intensity of transmitted light at a given wavelength is displayed. A time-resolution of 1 ns was used in the case of air-saturated samples. The start of the measurement is synchronized with the excitation pulse. There are shutters in the path of the excitation beam and in front of the probe lamp. To obtain a relevant decay curve of triplet states, three measurements are performed: 1) I_{L} is

the transmitted intensity when the lamp is opened and laser excitation shielded, 2) I_{F} is the intensity when the lamp is shielded and laser excitation opened, 3) I is the intensity when both are opened. The differential absorbance is then calculated as

$$\Delta A = \log_{10}\left(\frac{I_{\mathrm{L}}}{I - I_{\mathrm{F}}}\right). \tag{3.3}$$

Obtained ΔA kinetics were fitted by exponential decays. The linearity of ΔA amplitude on laser fluence was checked in the relevant fluence region.

3.5 Singlet Oxygen Phosphorescence

The phosphorescence of singlet oxygen at 1275 nm is very weak, as it is a spin-forbidden transition. A time-resolved measurement of emission after a short laser pulse excitation provides information about singlet oxygen lifetime and the dye triplet lifetime. The kinetics of decay can be also used for the evaluation of singlet oxygen quantum yield if an appropriate reference with known quantum yield is available.

The kinetics of singlet oxygen phosphorescence $I_{^1\mathrm{O}_2}(t)$ after a short laser-pulse excitation is the result of the convolution of dye-triplet decay function with singlet oxygen decay function. Both decays are considered monoexponential. The resulting kinetics is then

$$I_{^1\mathrm{O}_2}(t) \sim [\mathrm{T}_1]_0 \frac{1}{\tau_{\mathrm{T}}} \mathrm{e}^{-t/\tau_{\mathrm{T}}} * \mathrm{e}^{-t/\tau_{\Delta}} = \frac{[\mathrm{T}_1]_0\, \tau_{\Delta}}{\tau_{\Delta} - \tau_{\mathrm{T}}} (\mathrm{e}^{-t/\tau_{\Delta}} - \mathrm{e}^{-t/\tau_{\mathrm{T}}}), \tag{3.4}$$

where $[\mathrm{T}_1]_0$ is the number of triplets which give rise to singlet oxygen (and therefore the number of $^1\mathrm{O}_2$ molecules originated), τ_{Δ} is the singlet oxygen lifetime, and τ_{T} is the PS triplet lifetime. [5]. The function 3.4 can be fitted into the experimental data. The $[\mathrm{T}_1]_0$ parameter is proportional to the singlet oxygen quantum yield. For the investigated samples, singlet oxygen lifetimes are in the order of dozens of microseconds and triplet lifetimes are much shorter, in the order of hundreds of nanoseconds. Then, the rise-section of the kinetics can be approximated by exponential with the lifetime of the triplet and the decay-section by exponential with the lifetime of $^1\mathrm{O}_2$. The triplet lifetime is sometimes referred to as rise-time. However, for argon bubbled samples, the dominant quencher of triplets (oxygen) is depleted and the triplet-lifetime can significantly outgrow the lifetime of $^1\mathrm{O}_2$. The equation 3.4 remains valid, but the denominator is negative and the rise-time corresponds to singlet oxygen lifetime in this case.

Experimental setup. Triplet lifetimes and singlet oxygen lifetimes are typically much longer than those of fluorescence. As a result, the time-resolution doesn't need to be so high as in the case of TCSPC for fluorescence-lifetime measurements. An appropriate device for time-resolved phosphorescence is a multichannel scaler technique which allows to collect many photons in one laser period (in contrast to TCSPC).

A CryLas FTSS355-Q diode-pumped Nd:YAG pulsed laser was employed for excitation, working at 10 kHz repetition rate and delivering 1ns, 1.2µJ laser pulses. A gray-filter wheel is used for eventual attenuation of the laser in order to prevent some kind of saturation effects in the sample. The laser beam is

focused into a small spot in the sample cuvette. The emission from the sample passes through a set of lenses and an interference filter centered at 1275nm (filters centered at various wavelengths are available) and enters a Hamamatsu H9170-45 near-IR sensitive photomultiplier (cooled down to $-60°C$) working in photon counting mode. The signal is then conducted to a multichannel scaling board (PicoQuant's NanoHarp 200) through a preamplifier.

The principle of operation of a multichannel scaling board (MSB) will be described shortly. A detailed description of the technique is provided at [8]. A discriminator (described in section 3.3) delivers pulses to the MSB. In a basic configuration, the multichannel scaler switches through memory locations of high speed memory and drops discriminated pulses into the current location. The switching of addresses is driven by a quartz oscillator. The start of the sweep through the memory is synchronized with the excitation laser pulse. Many sweeps can be accumulated before the memory is read by the computer. The time-resolution of such a device is limited by the address switching rate. A device where discriminated pulses are fed into the shift register of length N and consequently processed in parallel, achieves a time-resolution down to about 1 ns. The memory directly contains the waveform of the signal [8].

The singlet oxygen quantum yield is calculated from parameter $[T_1]_0$ by fitting 3.4 into luminescence kinetics. The sample needs to have matched absorbance with a reference of known Φ_Δ (in our case TPP and C_{60}). The problem is that the inaccuracies of Φ_Δ of the reference compounds are estimated to be around $5-10\%$ [40]. It must be remembered that it's not possible to make a comparative measurement of two samples in different solvents, because oxygen solubility is strongly dependent on solvent. The operation frequency of 10 kHz (100 µs time period) is not convenient for measuring samples with long lifetimes of singlet oxygen because the phosphorescence signal from one period would reach to the next period. Singlet oxygen lifetimes of investigated samples are around 20 µs, are identical to those of the reference sample, and triplet lifetimes are in the range of hundreds of nanoseconds. Therefore, no significant signal built-up is present.

3.6 Delayed Fluorescence

The first excited singlet state of PS can be repopulated from triplet states

i) by interaction of two triplets, so called triplet-triplet annihilation

$$^3\mathrm{PS} +^3 \mathrm{PS} \rightarrow^1 \mathrm{PS}^* +^1 \mathrm{PS}\,,$$

ii) by interaction of the triplet with singlet oxygen

$$^3\mathrm{PS} + {}^1\mathrm{O}_2 \rightarrow^1 \mathrm{PS}^* +^3 \mathrm{O}_2\,,$$

iii) by a thermally activated radiationless transition.

The process (ii) is eliminated in argon or nitrogen saturated samples. Repopulated singlets emit delayed fluorescence (DF).

Let's suppose that DF is a minor channel of triplet decay. The triplet decay is considered monoexponential. The intensity of DF originated by process (i) is

quadratic in triplet concentration. Then, the lifetime of DF generated by process (i) is half of the triplet lifetime and the lifetime of DF generated by process (iii) is equal to the triplet lifetime. Kinetics of DF (the intensity of DF as a function of time after excitation laser pulse) can be fitted by the sum of two exponentials

$$I_{\mathrm{DF}}(t) = Ae^{-t/\tau_{\mathrm{T}}} + Be^{-2t/\tau_{\mathrm{T}}}\,, \tag{3.5}$$

where parameters A, B stand for initial rates of processes (iii), (i) respectively. The rate of process (i) strongly depends on the concentration of solute, light intensity and viscosity of the solvent. Two samples of the same concentration of solute at the same solvent will generally show different rates in different experimental devices due to different illumination conditions.

If the quadratic process (i) is not negligible as a channel of triplet decay, then the differential equation

$$\frac{\mathrm{d}[\mathrm{T}_1](t)}{\mathrm{d}t} = -a[\mathrm{T}_1] - b[\mathrm{T}_1]^2\,, \tag{3.6}$$

has to be solved to obtain a model of triplet kinetics. The equation is a Bernoulli equation with the solution

$$[\mathrm{T}_1](t) = \frac{1}{Ce^{at} - \frac{b}{a}}\,. \tag{3.7}$$

The problem is that a decay fitted by 3.7 may provide a non-negligible value of the ratio $b[\mathrm{T}_1]^2(0)/a[\mathrm{T}_1](0)$ while square residuals and fit-quality are nearly the same as for the monoexponential fit of the same decay.

DF was measured by a setup for transient absorption spectra. Samples were excited at 420 nm with $\sim$ 5 ns pulses (energy $\sim$ 5 mJ) from an optical parametric oscillator (PG122, EKSPLA) pumped by a Q-switched Nd:YAG laser (NL303G/TH, EKSPLA). The signal was detected by an intensified gated CCD camera (PI-MAX 512RB, Roper Scientific) coupled to an imaging spectrometer (Triax 320, Horiba Jobin Yvon). The whole spectrum is recorded by the CCD at a given time after the excitation pulse. Time-delay and time-width of the gate-window can be easily set with precision of one nanosecond. Detector sensitivity rapidly drops at the far-red and near-IR regions. The time-width of gate-window determines integration time. Decay kinetics can be obtained by measuring spectra for a series of time-delays with a narrow gate-window. However, a narrow gate-window leads to very poor detection efficiency which becomes a problem for weakly emitting samples. For wider gate-windows (Δt) it's necessary to adapt the model 3.5 resulting in

$$I_{\mathrm{DF}}(t) = \frac{A}{\tau_{\mathrm{T}}}e^{-t/\tau_{\mathrm{T}}}(1 - e^{-\Delta t/\tau_{\mathrm{T}}}) + \frac{B}{\tau_{\mathrm{T}}/2}e^{-2t/\tau_{\mathrm{T}}}(1 - e^{-2\Delta t/\tau_{\mathrm{T}}})\,. \tag{3.8}$$

Prompt fluorescence and delayed fluorescence (with a much longer lifetime) can be easily separated by shifting the time-delay. Quantum yields of prompt and delayed fluorescence can be compared by integrating the signals over corresponding time-regions. Thus it can be decided whether delayed fluorescence is a significant channel of triplet decay.

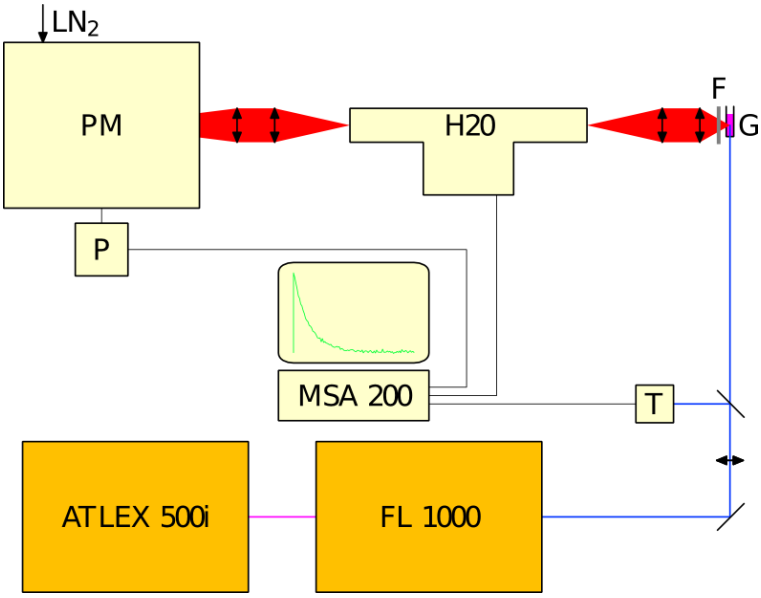

Figure 3.2: Experimental setup for time- and spectrally-resolved phosphorescence measurements of both PS and singlet oxygen

3.7 Photosensitizer Phosphorescence Spectrum

Phosphorescence of a photosensitizer is a spin-forbidden, very weak emission from the triplet state. The wavelength of the edge on the blue-most side of the spectrum corresponds to the energy of triplet state (0-0 transition). In liquids, collisional quenching of triplets leads to very poor phosphorescence quantum yields (usually less than 10^{-5}). The replacement of dissolved oxygen (an excellent triplet quencher) by an inert gas prolongs substantially the triplet lifetime and enhances phosphorescence quantum yield. The blue-side of the phosphorescence spectrum can be overlapped by extended fluorescence. Time- and spectrally-resolved luminescence measurement can easily distinguish between phosphorescence and prompt fluorescence (or another short lived processes) but the delayed fluorescence still may interfere.

The setup shown in figure 3.2 was used to detect weak phosphorescence of the investigated samples (see the detailed description at [19]). Excimer laser ATLEX-500i (ATL Lasertechnik) pumps the pulsed dye laser FL1000 (Lambda Physik, dye Stilben 3), emitting pulses at 420 nm (Soret of TPP) of 7 ns time-width, energy of about 20 µJ, and repeat-frequency of 400 Hz. The PIN diode (T) synchronizes the measurement period with a laser pulse and at the same time allows to measure laser energy. The signal from the quartz cuvette (C) is collected by the lens assembly and passes through a pair of Schott RG7 long-pass filters (F, transmittance shown in figure 3.3) and through the monochromator Jobin-Yvon H20IR (H20). The signal is detected by the IR-sensitive photomultiplier Hamamatsu R5509 (PM) cooled down to −80 °C operating in a single photon counting mode. The output of the photomultiplier is preamplified and counted by the multi-scaler Becker-Hickl MSA 200 with 5 ns per channel.

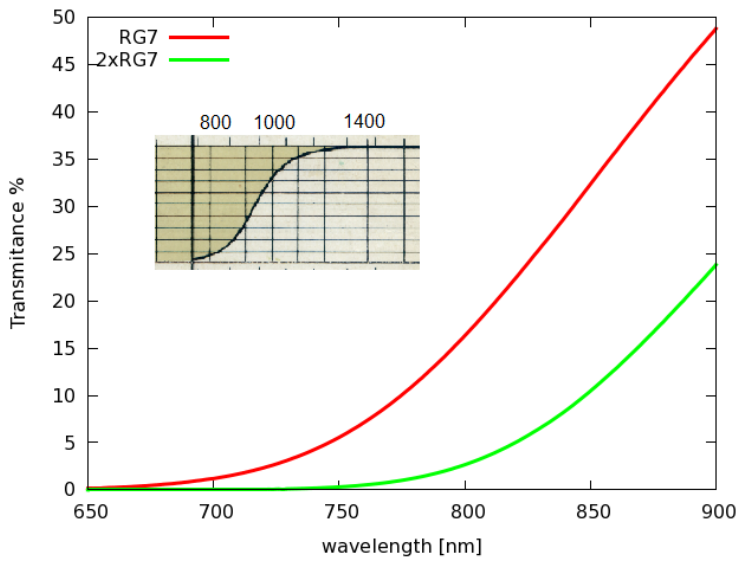

Figure 3.3: Transmittance of Schott RG7 long-pass filter. Data provided by manufacturer are displayed at the inset.

3.8 Laser-induced Optoacoustic Spectroscopy

Laser induced optoacoustic spectroscopy is a calorimetric method which can be used for the determination of triplet and singlet oxygen quantum yields in solutions of photosensitizers. The sample is excited by nanosecond laser pulse. A part of the absorbed energy is dissipated as heat during the time when the excited state non-radiatively relaxes through various pathways and intermediates. The transition from excited to ground state induces heat release and structural changes in the solution giving rise to pressure changes detected by a microphone. A time-resolved measurement of pressure changes gives information about lifetimes and quantum yields of emergent intermediates. Calorimetric standards are very well defined which is an important advantage when compared to the luminescence based methods for singlet oxygen quantum yields measurements. The following text refers only to simple solutions of porphyrins. General concepts of optoacoustic methods are covered in [9, 24, 26].

3.8.1 Separation of Structural and Thermal Volume Changes

Pressure (acoustic) wave is a result of either structural volume changes (ΔV_S) or a thermal expansion of the sample solution. In this work, structural volume change refers to the change between the *ground* singlet and the first excited triplet of chromophore. Structural volume changes of porphyrins in polar solvents (e.g. water) are believed to be dominated by rearrangement of solvent and solute molecules driven by alteration of dipole-dipole interaction or hydrogen-bonding [25, 26]. The ΔV_S is much smaller for non-polar solvents and is assigned to intrinsic contraction – change of bond lengths – in the excited state [25]. The structural volume change ΔV_S is usually measured in $Å^3$ per each molecule of solute.

In order to combine the structural and thermal contribution to the acoustic signal, the thermal contribution will be expressed as a volume change per one

solute molecule too. For simplicity let's suppose that a molecule immediately releases absorbed energy E_a as heat. Temperature change ΔT of the whole sample due to heat release from one molecule is given

$$\Delta T = \frac{E_\mathrm{a}}{c_\mathrm{p}\rho V}\,, \tag{3.9}$$

where c_p is the heat capacity per unit of mass of the solvent, ρ density of the solvent and V volume of the sample solution. The thermal expansion coefficient β is defined

$$\beta = \frac{1}{V}\left(\frac{\partial V}{\partial T}\right)_p\,. \tag{3.10}$$

The resulting thermal volume change of the whole sample per one solute molecule is then

$$\Delta V_\mathrm{T} = V\beta\Delta T = \beta\frac{E_\mathrm{a}}{c_\mathrm{p}\rho}\,. \tag{3.11}$$

In order to determine quantum yields from optoacoustic measurements, one has to know how big the structural contribution is when compared to the thermal one. Structural volume change can be readily determined in water solutions by measuring acoustic amplitude upon different temperatures, because water shows strong dependence of the thermal expansion coefficient on temperature. Moreover, water has density maximum around 4°C which means that the thermal expansion coefficient β equals zero for this temperature and the contribution of the thermal volume change vanishes [24]. Nevertheless, dependence of β on temperature is generally much weaker for majority of common organic solvents and separation of structural and thermal changes cannot be easily performed. One possible way of measuring ΔV_S of solute in non-polar organic solvents is to prepare a heterogeneous water solution containing droplets of a non-polar solvent. Structural volume change of $-4\,\text{Å}^3$ was determined for TPP incorporated in Triton X-100 hydrophobic micelle environment. Values around $-18\,\text{Å}^3$ were obtained for various differently substituted ionic porphyrins in water (e.g. $\mathrm{TPPS_4}$). The structural volume change decreased to $-4\,\text{Å}^3$ upon low pH for fully protonated forms of these porphyrins [25]. A similar decrease was observed as a result of dimer formation or metal complexation. Generally, such a decrease seems to be caused by blocking hydrogen-bond interactions of solvent with core-nitrogens. These results suggest that the structural contraction of about $-4\,\text{Å}^3$ can be attributed to intrinsic contraction of the porphyrin ring in excited state while the larger contribution of about $-14\,\text{Å}^3$ can be attributed to stronger hydrogen-bond interactions between solvent and the porphyrin-core in excited state. The character of meso-substituents is not markedly involved in the generation of structural volume change [25].

Typical thermal volume change can be readily estimated. Table 3.1 summarizes thermal properties of chosen solvents. Coefficients β are slightly above $10^{-3}\mathrm{K}^{-1}$ for a wide range of organic solvents while they are five-fold smaller for water. On the contrary, the heat capacity of organic solvents is typically few-fold smaller than that of water further increasing the value of the β/c_p term. Organic solvents therefore prove to give much a stronger signal arising from thermal volume changes when compared to water. For toluene and 532 nm excitation we

	β $[10^{-3} \cdot \mathrm{K}^{-1}]$	c_p $[\mathrm{J} \cdot \mathrm{g}^{-1} \cdot \mathrm{K}^{-1}]$	ρ $[\mathrm{g} \cdot \mathrm{cm}^{-3}]$
water	0.19^a	4.19^a	1.00^a
toluene	1.08^a	1.70^a	0.86^a
THF	1.26^d	1.72^b	0.88^b
DMF	1.01^c	2.06^b	0.94^b

Table 3.1: Thermophysical properties of selected solvents. ^{a} taken from [9], ^{b} taken from [36], ^{c} taken from [21], ^{d} taken from Invista product sheet.

get

$$\Delta V_\mathrm{T} = \beta \frac{E_\mathrm{a}}{c_\mathrm{p}\rho} \approx 200\,\mathrm{\AA}^3 \tag{3.12}$$

per one molecule of solute. The value is similar for THF and DMF (see table 3.1).

The structural volume change of Thiazolyl-porphyrins and TPP is supposed to be around $-4\,\mathrm{\AA}^3$ in toluene, since toluene is non-polar and doesn't form hydrogen bonds. It means that the structural volume change contributes only by 2% to the overall acoustic signal. THF and DMF are polar aprotic solvents able to form hydrogen bonds. Therefore, the contribution of ΔV_S may be higher than 2% in THF and DMF solutions.

This section implies a very important conclusion: Both TPP and Thiazolyls in toluene are supposed to show structural contribution of maximally few percents. Solutions in THF and DMF may show a larger contribution of ΔV_S and it has to be taken into account especially during the interpretation of triplet quantum yield measurements.

3.8.2 Experimental Setup

The principle of experimental setup is shown in figure 3.4 and the method is described in [38]. An OPO pulsed laser light (5 ns pulse width) attenuated by appropriate gray filters passes through the slit into the sample cuvette exciting rectangular volume (better than cylindrical [24]). The microphone is attached to the cell wall in right angle geometry. The signal from the microphone is amplified and recorded by a digital oscilloscope with a time resolution of 10 ns. A fraction of the excitation beam is directed into an energy-meter. The energy of the incident excitation laser pulse is typically in the range $1-20\,\mu\mathrm{J}$ (the energy-meter doesn't measure the absolute energy of the incident excitation pulse, but is able to detect the drift of the pulse energy). Time-dependent acoustic signal recorded by the microphone is considered to be a convolution of instrument response function $\mathrm{IRF}(t)$ with monoexponential decays which correspond to decays of the intermediate states. Such time-resolved measurement allows us to determine and distinguish fractions of absorbed heat released in processes with different lifetimes. $\mathrm{IRF}(t)$ is obtained as a response for calorimetric reference which immediately (in sub-nanosecond time scales) releases 100% of the absorbed energy as heat (e.g. azulene for 532nm excitation and hydroxy-benzophenone for 355nm). A typical signal from optoacoustic measurement is shown in figure 4.9 in section 4.6. All

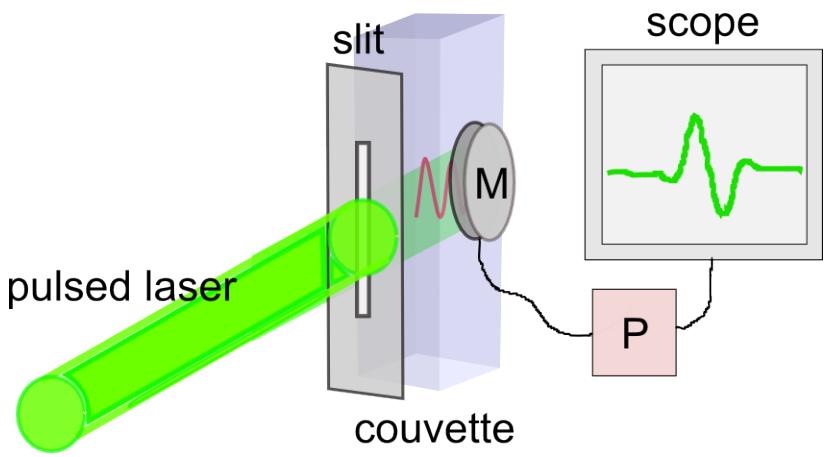

Figure 3.4: Principle of optoacoustic measurement. (M) is a microphone and (P) is a preamplifier.

the samples and the reference have to be measured in the same cuvette without changing its position, because even a subtle change in experiment geometry strongly changes shape of the IRF(t). One has to be especially careful while replacing the sample solution from the cuvette in order to preserve the experiment geometry. All the samples and reference need to have matched absorbances at the excitation wavelength. Absorbance at the excitation wavelength (532 nm) was matched to 0.1 which corresponds to concentrations of about 20 µM for observed compounds. The experiment should be carried out in the region of linear dependence of the acoustic signal on laser fluence, which is achieved by rotating the gray-filter wheel.

3.8.3 Quantum Yields of Singlet Oxygen and PS Triplet

Our model of the photosensitization of singlet oxygen is described at scheme 2.2. Three intermediate states are present. The excited singlet state decays with lifetimes of a few nanoseconds as learned from fluorescence lifetimes and heat released will be referred to as fast heat. The triplet population is built up very quickly and decays with a lifetime of hundreds nanoseconds depending on the solvent and oxygen concentration. Resulting heat release will be referred to as slow heat. Finally, singlet oxygen is populated and decays with lifetimes of dozens of microseconds. However, heat released in processes with a lifetime longer than 10 µs is practically undetectable by the system and energy trapped in singlet oxygen is referred as stored heat [38, 46]. Some part of the absorbed energy is released in radiative processes (fluorescence and phosphorescence) and is invisible for optoacoustic spectroscopy. The fluorescence quantum yield has to be known in order to determine Φ_{T} and Φ_{Δ}. The phosphorescence quantum yields in solutions at normal temperatures are typically smaller than 10^{-5} and are neglected. The fraction of absorbed energy released as fast heat and slow heat is determined by fitting $f(t)$ into the signal, where

$$f(t) = \mathrm{IRF}(t) * \frac{q_1}{\tau_{\mathrm{S}}} \mathrm{e}^{-t/\tau_{\mathrm{S}}} + \mathrm{IRF}(t) * \frac{q_2}{\tau_{\mathrm{T}}} \mathrm{e}^{-t/\tau_{\mathrm{T}}} \,. \tag{3.13}$$

Fit-parameters q_1, q_2 stand for the fraction of absorbed energy released as fast and slow heat respectively. The parameter τ_T corresponds to triplet lifetime and should be fixed to the value obtained by flash-photolysis. The parameter τ_S corresponds to the lifetime of the excited singlet and should be fixed to the value obtained by the fluorescence lifetime measurement. The first term in 3.13 effectively reduces to $q_1\mathrm{IRF}(t)$ in the case that τ_S is short compared to time-resolution. The data were processed by an Octave program which is presented in the Attachment.

Scheme 3.5 shows how fit-parameters q_1, q_2 are related to Φ_T, Φ_Δ and excited state energies. The idea of the scheme is that the energy released in each decay between two states equals the area of a rectangle with width corresponding to quantum yield and height corresponding to the energy difference between the two states. The sum of areas of rectangles corresponding to all forms of decay has to equal the area of the rectangle corresponding to absorbed energy. It implies

$$E_\Delta \Phi_\Delta = E_\mathrm{a}(1 - q_1 - q_2) - E_\mathrm{F}\Phi_\mathrm{F} \tag{3.14}$$

$$E_\mathrm{T}\Phi_\mathrm{T} = E_\mathrm{a}(1 - q_1) - E_\mathrm{F}\Phi_\mathrm{F}\,. \tag{3.15}$$

The advantage of the first equation is the following: The triplet energy of PS needn't to be known and moreover, the effect of structural volume change of the PS triplet vanishes (see section 3.8.4). The second equation requires knowledge of the triplet energy and the structural volume change of the PS triplet has to be considered. The second equation is valid also for argon- and nitrogen-saturated samples where no energy transfer to singlet oxygen takes place and triplet lifetime prolongs, such that heat is stored in PS triplets instead of in singlet oxygen.

3.8.4 Obstacles

There are a few important obstacles which prevent the optoacoustic spectroscopy from being more precise than approximately 5%. In order to obtain more precise values of quantum yields, some measures and new approaches were employed.

1) Despite working in the region of linear dependence of signal amplitude on laser fluence, there is a remarkable decreasing trend in the dependence of Φ_Δ on laser fluence for higher energies. Therefore a new approach is used – the dependence of Φ_Δ on laser fluence was measured for all samples.

2) As shown from equation 3.14, the resulting Φ_Δ is obtained from term $(1 - q_1 - q_2)$, which typically equals ≈ 0.35 for investigated compounds. The relative error of q_1, q_2 leads to a doubled error in Φ_Δ. If there is a mismatch between absorbances of the sample and the reference (or mismatch between excitation energies), parameters q_1, q_2 have to be multiplied by the factor

$$E_\mathrm{ref}(1 - 10^{-A_\mathrm{ref}})/E_\mathrm{sam}(1 - 10^{-A_\mathrm{sam}})\,. \tag{3.16}$$

3) Wavelength-shift of a few tenths of a nanometer can cause remarkable change in absorbance of the sample. The absorbances of the samples and reference solutions were matched at excitation wavelength with use of the absorption spectrometer. Nevertheless, the real absorbances of the samples and the reference may be up to 10% mismatched at the excitation wavelength (due to a slightly shifted calibration of the spectrometer, or unequal shape of spectral transmissivity of the spectrometer and spectral shape of the excitation laser light). In

order to cancel the error caused by absorbance mismatch, Φ_T can be calculated by means of the ratio q_1/q_2 in the following way

$$\Phi_\mathrm{T} = \frac{E_\mathrm{a} - \Phi_\mathrm{F} E_\mathrm{F}}{\frac{q_1}{q_2}(E_\mathrm{T} - pE_\Delta) + E_\mathrm{T}}\,, \tag{3.17}$$

where p is a fraction of triplets quenched by energy transfer to singlet oxygen. Inaccuracy of Φ_T calculated from 3.17 is a combination of the uncertainty of triplet energy and uncertainty of parameter p. Structural volume changes are not taken into account. Nevertheless, if p is supposed to be close to unity and structural volume changes are negligible, the later equation can provide meaningful results.

4) The equations 3.14, 3.15, and 3.17 were derived under the assumption that $q_{1,2} = \Delta V_\mathrm{T}^{(1,2)}/\Delta V_\mathrm{T}^\mathrm{ref}$, where $\Delta V_\mathrm{T}^{(1,2)}$ are thermal volume changes corresponding to fast and slow heat releases and $\Delta V_\mathrm{T}^\mathrm{ref}$ is the thermal volume change of the reference sample. Actually, structural changes upon triplet formation interfere and therefore $q_{1,2} = (\Delta V_\mathrm{T}^{(1,2)} + \Delta V_\mathrm{S}^{(1,2)})/\Delta V_\mathrm{T}^\mathrm{ref}$. In order to obtain correct results for quantum yields, terms q_1, q_2 in equations 3.14, 3.15, 3.17 should be replaced by terms

$$\widetilde{q}_{1,2} = q_{1,2} - \frac{\Delta V_\mathrm{S}^{(1,2)}}{\Delta V_\mathrm{T}^\mathrm{ref}}\,,$$

The term $\Delta V_\mathrm{S}^{(1)}$ stands for the volume change upon transition from the ground state to triplet state and is negative for investigated compounds. Analogically, the term $\Delta V_\mathrm{S}^{(2)}$ stands for the volume change upon transition from the triplet state to ground state and is positive for investigated compounds ($\Delta V_\mathrm{S}^{(1)} = -\Delta V_\mathrm{S}^{(2)}$). The equation 3.14 remains unchanged after this correction and is valid even if ΔV_S is present. On the contrary, equations 3.15 and 3.17 are affected. This correction hasn't been employed for calculations of experimental results, because the value of ΔV_S is not rigorously known. However, it's a useful guide for the consideration of the accuracy of experimental results. Structural volume changes upon excited singlet formation do not affect experimental results because reverse changes occur consecutively upon the decay of the excited singlet.

5) Fit-parameters q_1, q_2, τ strongly correlate. Parameter τ should be fixed to the value of triplet lifetime obtained by flash-photolysis.

6) There can be a difference between the speed of sound in the sample and reference solution. The difference may be caused by unequal concentrations or temperatures of the solutions. Therefore, shift fit-parameter t_0 should be employed (which means the substitution of $\mathrm{IRF}(t)$ by $\mathrm{IRF}(t - t_0)$ in 3.13). It was estimated that the time-shift parameter shouldn't significantly exceed the range $0 - 20\,\mathrm{ns}$ (the width of two channels). The time-shift parameter also covers some minor disturbances in experiment geometry. Time-shift parameter correlates with the other fit-parameters and should be minimized.

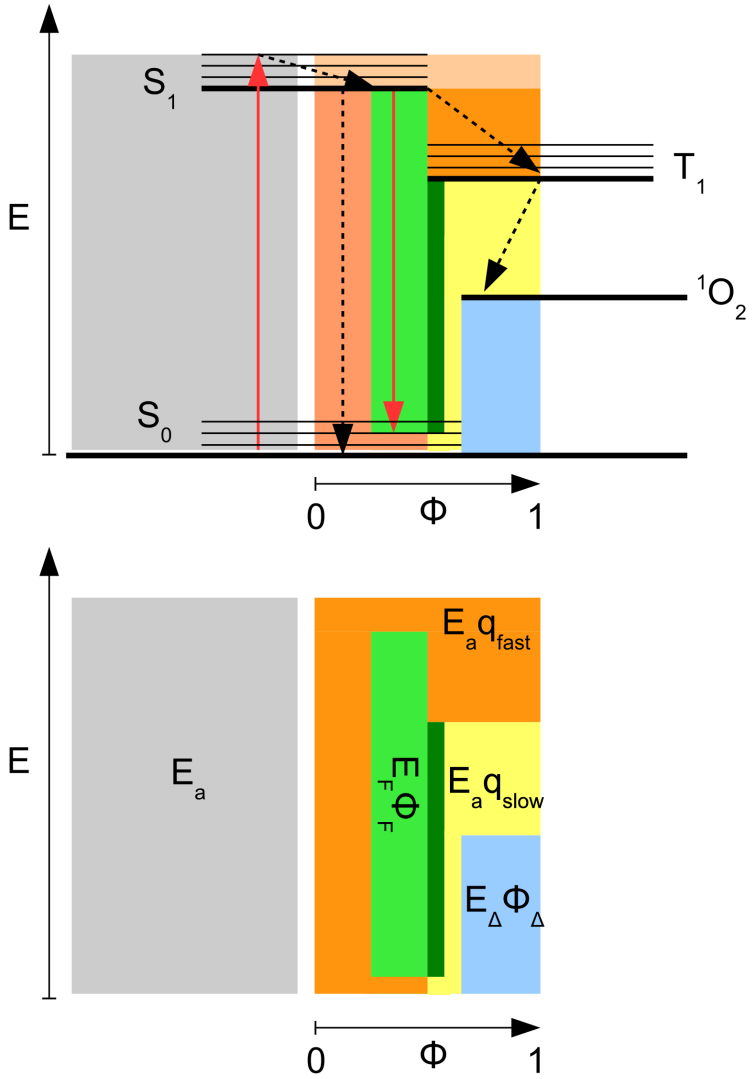

Figure 3.5: Calorimetric processes in optoacoustic spectroscopy. Black arrows stand for non-radiative transitions, red ones for radiative transitions. Orange areas correspond to fast heat release in the time range of nanoseconds or shorter. Green areas correspond to fluorescence and phosphorescence, nevertheless the phosphorescence is considered to be absolutely negligible. Yellow areas stand for slow heat release in the time range of hundreds of nanoseconds. Blue area denotes the so-called stored heat – heat released in processes with lifetimes longer than about 10 µs which are not visible for the apparatus.

3.9 Microscopy

In recent years, great efforts have been made to develop microscopic techniques to observe singlet oxygen phosphorescence directly in living cells with subcellular-resolution and sufficient sensitivity (especially many works published by group of prof. Ogilby, for example [44]). Such microscopic observations would, among others, elucidate mechanisms of the photosensitization process and singlet oxygen action in living cells.

Eucaryotic cells are typically of the size $10 - 30\,\mu m$. Spatial resolution can be achieved by scanning the sample by a focused laser beam while emission is de-

tected by a PMT in single-photon counting mode (similarly to the setup described in 3.7). The size of the focus spot is diffraction limited and can be practically decreased down to a few micrometers. Better spatial resolution can be achieved with confocal methods or multi-photon excitation methods. The disadvantage of scanning techniques is the need for a long scan-time which is not compatible with real-time biological experiments. Another approach is a classical luminescence microscope combined with a near-IR sensitive 2-D semiconductor detector array (e.g. classical CCD cameras). Spatial resolution is determined by the ratio of detector-pixel size and objective magnification and, of course, is diffraction limited, too. Low photon fluxes through each pixel carry the necessity of a very sensitive detector array with a good signal-to-noise ratio. Current detector technology already allows for the creation of useful singlet-oxygen-based images. The intensity of singlet oxygen emission can be substantially increased by replacing H_2O with D_2O in cell samples ($\tau_\Delta(H_2O) = 3,5\,\mu s$ and $\tau_\Delta(D_2O) = 68\,\mu s$). A nice review of microscopic techniques is provided at [44].

In our lab, 2-D detector-array based microscopy techniques are currently being developed. The worldwide unique experimental setup with both VIS and near-IR cameras allowing observation of both visible PS fluorescence and infrared-phosphorescence imaging is shown in figure 3.6. A continual laser at 405 nm excites the sample at the Soret band of PS. Objectives (O) of 4×, 20× and 50× magnifications are available. Emission light passes through a dichroic mirror (D) which cuts off shorter wavelengths. A set of dichroic mirrors is available – a mirror with an edge around 750 nm is used for phosphorescence measurements and a mirror with edge around 450 nm is used for fluorescence. If a golden mirror (M) is placed then the signal beam is directed toward the IR-camera, otherwise is directed toward the VIS-camera. In the IR-branch, the signal passes through two long-pass RG7 filters (see transmittance in figure 3.3) in order to cut off fluorescence, and consequently passes through a polychromator (Sp). The near-IR-sensitive intensified CCD camera Mosir 950 collects the signal. If the grating is set to zero-order diffraction then normal image can be observed. Spectral sensitivity of the camera is declared to be remarkably better than that of a traditional InGaAs detector (shown in figure 3.7). Sensitivity for wavelengths under 900 nm is very low which is favourable for the suppression of fluorescence. Camera allows for a gating mode which potentially could be used together with a pulsed laser to cut off short-lived fluorescence and scattering. The drop of camera sensitivity, two RG7 filters and the dichroic mirror all lead to the suppression of fluorescence transmitted compared to phosphorescence. However, fluorescence quantum yields are many orders of magnitude bigger than phosphorescence quantum yields. Therefore, an eventual overlap of phosphorescence and fluorescence at the resulting image still must be considered.

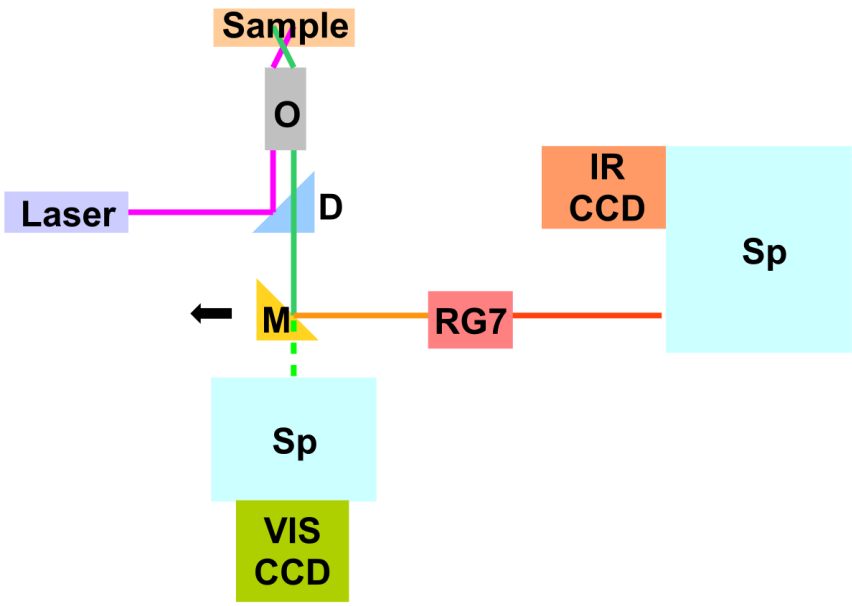

Figure 3.6: Experimental setup for both the fluorescence and phosphorescence microscopic imaging.

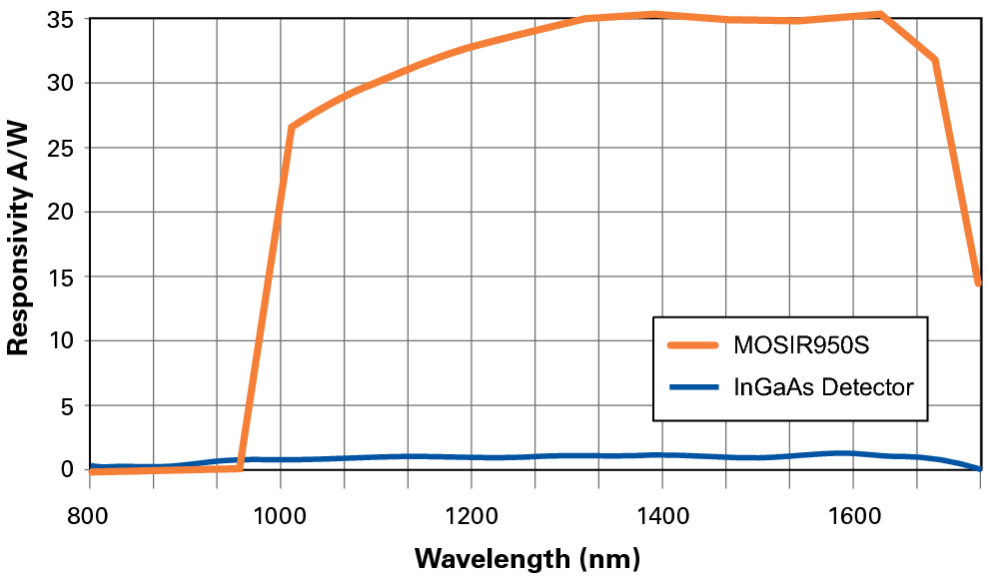

Figure 3.7: Spectral sensitivity of Mosir 950 camera compared to traditional InGaAs array (from [32]).

4 Results and discussion

4.1 Solubility

Thiazolyls are less soluble than TPP. DMF showed to be the best for Thiazolyls from tested solvents. Toluene and THF are satisfactory as well. However, the highest achieved concentrations were around 25 µM. The solubility is illustrated at diagram 4.1. The solubility was qualitatively tested by dipping a Pasteur pipette with few crystals of material into the solvent. A quick melt means good solubility.

4.2 Absorption Spectra

The formal replacement of phenyl groups in TPP by four thiazole or bithiazole groups does not change principal characteristics of the absorption spectrum (figure 4.2), but induces a bathochromic shift of 8 nm (Soret band) and 17 nm (lowest-energy Q-band). It suggests that these heterocycles exert a different electronic perturbation. There is no difference in the shape of spectra between the two Thiazolyls, but BiThiazolyl shows significantly higher extinction coefficients. Extinction coefficients in the Soret band of $4.6 \cdot 10^5$, $1.9 \cdot 10^5$ and $2.6 \cdot 10^5\,\mathrm{M^{-1}cm^{-1}}$ were obtained for TPP, MonoThiazolyl and BiThiazolyl respectively. Absorption of TPP in the Soret band is approximately twice as strong as that of the Thiazolyls. The extinction coefficients of BiThiazolyl and TPP are comparable in Q-bands (around $5 \cdot 10^3\,\mathrm{M^{-1}cm^{-1}}$). The concentration dependence of absorbance is plotted in figure 4.3. The dependence is linear in the frame of experiment accuracy. Non-linearity would reveal a presence of aggregation. The linearity of concentration dependence of the absorbance was qualitatively checked at concentrations up to about 10 µM for Thiazolyls in THF (data not shown).

Photobleaching of Thiazolyls and TPP were previously investigated by the group of Dr. Santi Nonell. Photostabilities of Thiazolyls and TPP are almost identical. Fullerene C_{60} was used as a highly photostable control compound.

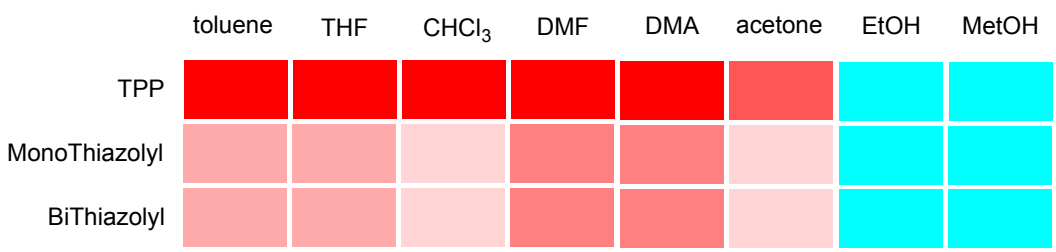

Figure 4.1: Solubility of TPP and Thiazolyls in various organic solvents. Vivid red means good solubility, pale pink bad solubility and sky-blue refers to insolubility.

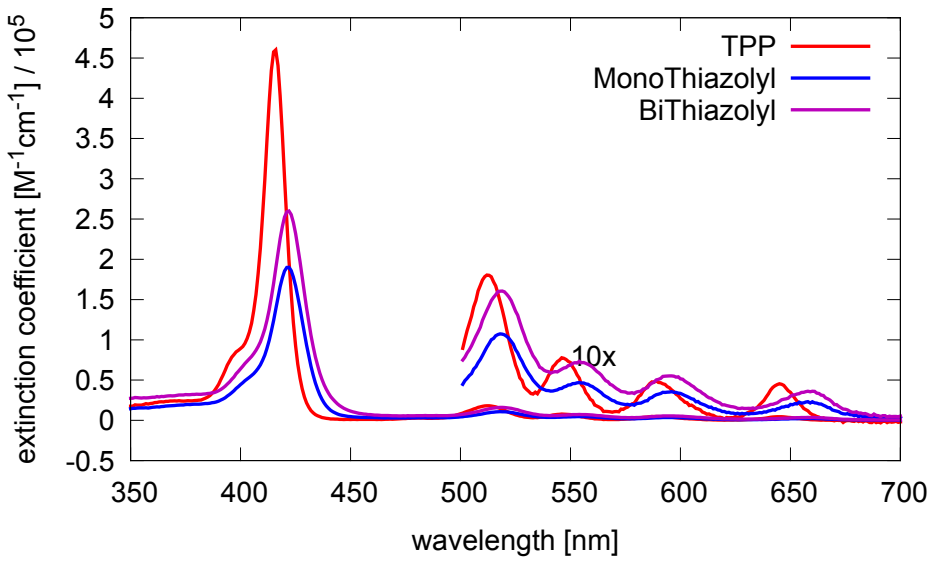

Figure 4.2: Absorption coefficients of TPP and Thiazolyls in DMF.

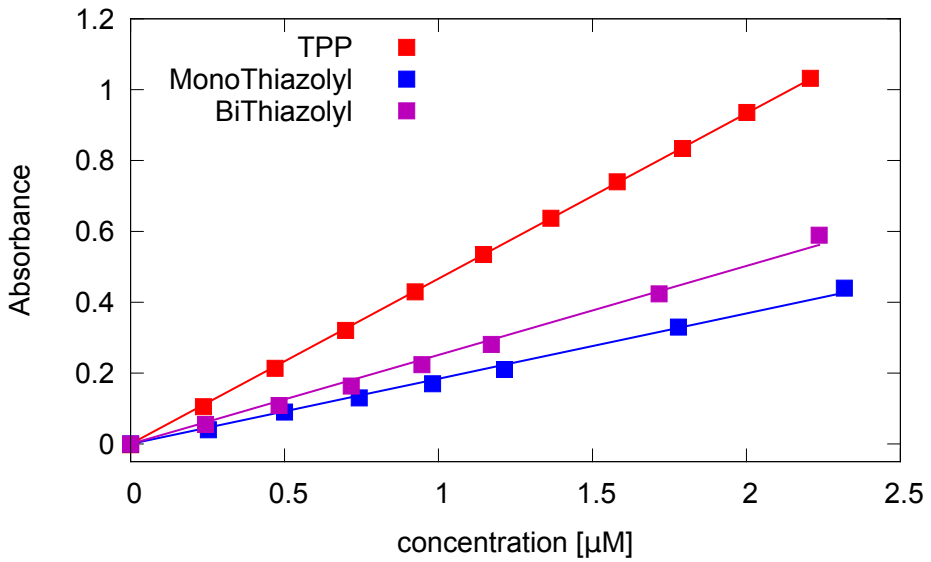

Figure 4.3: Concentration dependence of absorbance for TPP and Thiazolyls in DMF.

4.3 Fluorescence

The electronic perturbations revealed in the absorption spectra are also apparent in the fluorescence behaviour of the three compounds. The emission spectra of Thiazolyls show the expected bathochromic shift of about 16 nm (figure 4.5). The shift corresponds well with the shift of the lowest-energy Q-band. Likewise, the fluorescence quantum yields (Φ_F) of Thiazolyls are an order of magnitude smaller than Φ_F of TPP (11% for TPP while approximately 1% for Thiazolyls). The bright red fluorescence of TPP can be seen by naked eye upon irradiation by blue laser or UV lamp while Thiazolyls don't show any.

Fluorescence decays of TPP and Thiazolyls were fitted by the convolution of laser pulse time-shape with one exponential (figure 4.4). Biexponential fit didn't markedly improve the quality of the fit. Fluorescence lifetimes (τ_S) of Thiazolyls result 1.5 ± 0.2 ns (table 5.1) and are substantially shorter than that of TPP (~ 10 ns). Non-radiative decay processes are enhanced for Thiazolyls. Indeed, the rate constants for all non-radiative processes, calculated as $k_{NR} = (1-\Phi_F)/\tau_S$, increase roughly by a factor of 7.

4.4 Triplet Lifetimes and T-S Absorption

The triplet lifetimes of Thiazolyls and TPP were measured in air-saturated samples (DMF, THF and toluene), argon-saturated samples (DMF, THF) and oxygen-saturated samples (DMF) by flash-photolysis. Triplet decay kinetics were satisfactorily fitted by one exponential. Triplet lifetimes of TPP results 480 ± 10 ns in air-saturated DMF while lifetimes of MonoThiazolyl and BiThiazolyl result 400 ± 10 ns and 410 ± 10 ns respectively (figure 4.6). Triplet lifetimes of TPP are approximately 20% higher than for Thiazolyls in all air-saturated solvents (table 5.1). A significant difference between TPP and Thiazolyls was found for lifetimes in argon-saturated samples. TPP triplet lifetimes in argon-saturated sample are higher than 200 µs, while both Thiazolyl-triplets have lifetimes of 50 ± 10 µs both in DMF and THF. Despite the difficulty of preparing properly de-oxygenated samples, the lifetimes were reproducible within the stated accuracy. The absence of oxygen was checked by measuring its luminescence at 1275 nm. The lifetimes of Thiazolyl-triplets in argon-saturated samples obtained from time-resolved luminescence measurement are in perfect correspondence. The largely prolonged lifetime proves that interaction with oxygen is by far the most important decay channel of PS triplets. Lifetimes of oxygen-saturated samples turned out to be around 0.1 µs. This result agrees with expectations, because oxygen concentration in an oxygen-saturated sample is approximately four-fold higher than in an air-saturated one. However, relatively high inaccuracy due to a weak signal doesn't allow us to make any further judgement. The triplet-minus-singlet absorption spectrum was recorded as well (figure 4.7). Triplet kinetics were recorded in the spectral range from 400 nm to 650 nm. The value of fit-function at zero time is plotted. The inversed peak around 420 nm corresponds to Soret absorption band. The band of positive ΔA corresponds to triplet-triplet absorption. The maximum of triplet absorption was found to be around 470 nm for Thiazolyls and around 450 nm for TPP.

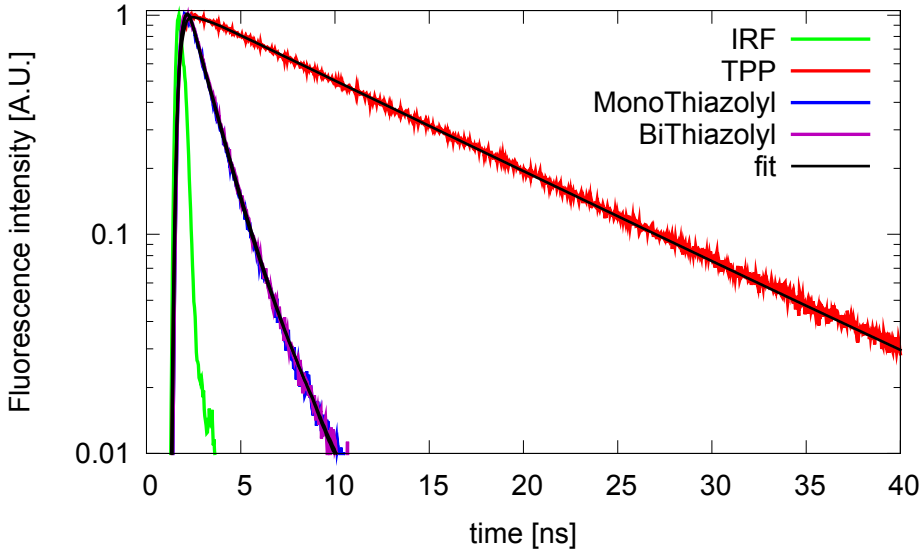

Figure 4.4: Fluorescence decays of TPP and Thiazolyls in DMF. The signal was fitted by a convolution of the excitation pulse shape with monoexponential decay.

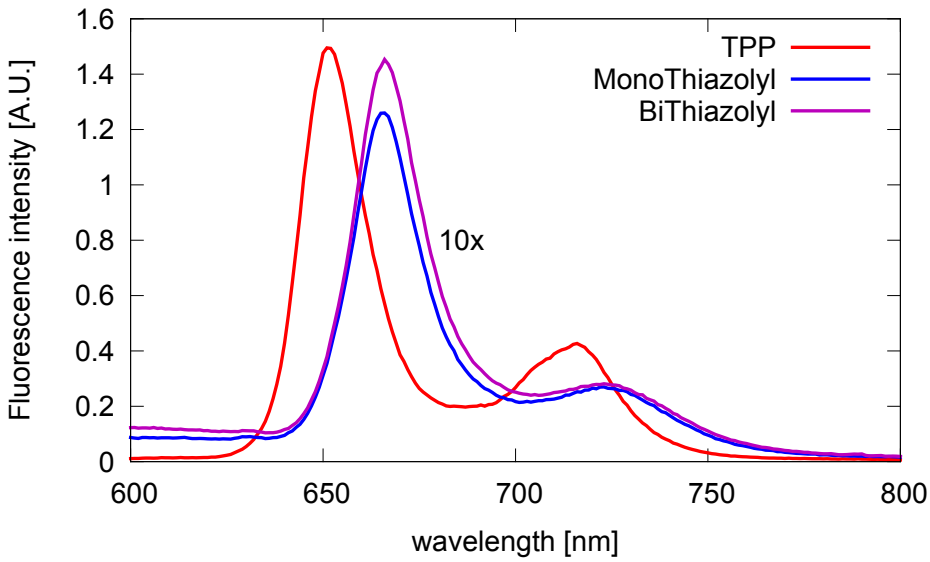

Figure 4.5: Fluorescence spectra of TPP and Thiazolyls in THF. Spectra of Thiazolyls are multiplied by factor 10.

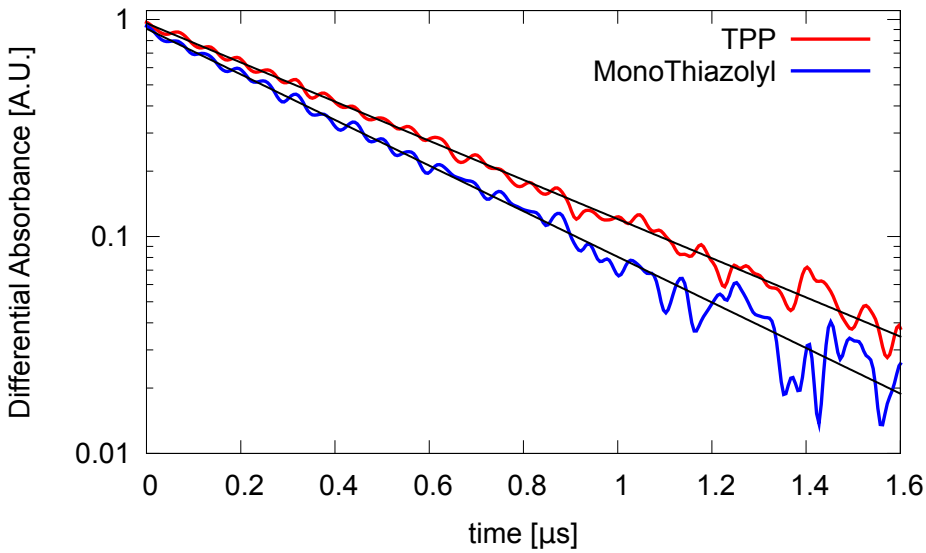

Figure 4.6: Normalized triplet decay of TPP and MonoThiazolyl in air-saturated DMF fitted by one exponential.

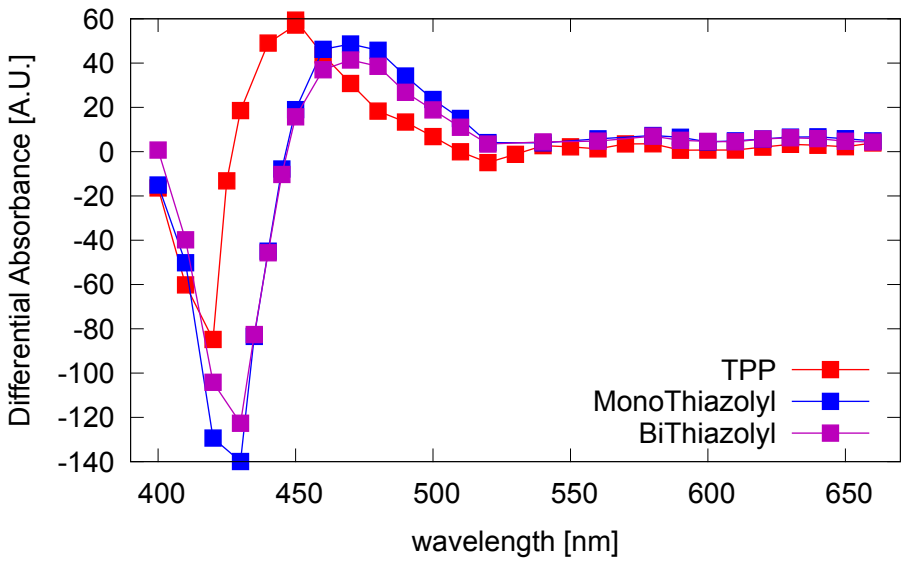

Figure 4.7: Triplet minus singlet absorption spectra of TPP and Thiazolyls in DMF measured by flash-photolysis.

4.5 Singlet Oxygen Production

Quantum yields of singlet oxygen were measured by the apparatus described in section 3.5. Phosphorescence kinetics were fitted by function 3.4. The quantity $[T_1]_0$ corresponds to the amount of triplets which give rise to singlet oxygen and thus is proportional to the singlet oxygen quantum yield. TPP was used as a reference compound with $\Phi_\Delta = 0.65 \pm 0.05$ and fullerene C_{60} with $\Phi_\Delta \approx 1.0$ was used as a control [40, 50].

Singlet oxygen lifetimes are the same for all compounds, 21 ± 1 µs in THF and DMF, and 29 ± 1 µs in toluene. Rise-times of singlet oxygen luminescence correspond to triplet lifetimes obtained by flash-photolysis (see section 4.4 and table 5.1). The intensity of the singlet oxygen phosphorescence signals (at 1275 nm) is markedly higher for Thiazolyls than for TPP and comparable to that of C_{60} (4.8). Singlet oxygen quantum yields of both Thiazolyls are basically the same. The Φ_Δ values for Thiazolyls were determined to be 0.80 ± 0.10 (TPP as a reference). Particular values are summarized in table 4.1. Relatively large uncertainty arises mainly from inaccuracy of Φ_Δ of the reference. If C_{60} taken as a reference, the Φ_Δ of Thiazolyls comes out to be very close to 1.0. The problem with this comparative method is the fact that quantum yields of references are not well defined. Quantum yields of singlet oxygen production were also measured by aptoacoustic spectroscopy, which is discussed further in the text.

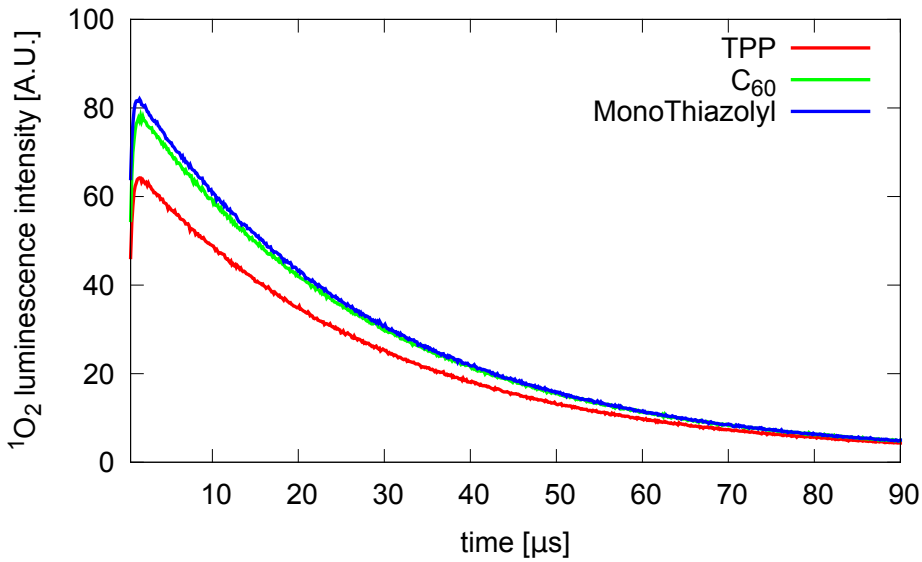

Figure 4.8: Singlet oxygen luminescence of TPP, MonoThiazolyl and C_{60} in toluene.

4.6 Quantum Yields by Optoacoustic Spectroscopy

The setup described in section 3.8.2 was used for optoacoustic measurements. The data were handled according to sections 3.8.3 and 3.8.4. Samples were excited at 532 nm. A typical signal from optoacoustic experiment is shown in figure 4.9.

A new approach for evaluating Φ_Δ and Φ_T was used. The dependences of the resulting Φ_Δ and Φ_T on laser fluence were measured (incident laser pulse energies were approximately in the range $1 - 20\,\mu J$). Besides checking that data were acquired in the region of linearity of the signal amplitude on laser fluence, the new approach assures that only relevant data will be taken into account.

Quantum yields Φ_Δ were computed according to the equation 3.14. Figure 4.10 shows the fluence dependence of computed Φ_Δ values of TPP, MonoThiazolyl and C_{60} in toluene for 532 nm excitation. Higher laser fluences obviously disturb linearity and respective values are not taken into account for further calculations. Quantum yields of singlet oxygen production for Thiazolyls determined by optoacoustic spectroscopy turn out to be close to unity for all used solvents, namely 0.9 ± 0.1. The values are summarized in table 4.1. There is no significant difference between the two Thiazolyls in the frame of experiment accuracy. The Φ_Δ of TPP was determined to be 0.59 ± 0.06 in toluene and 0.66 ± 0.06 in both THF and DMF, and Φ_Δ of C_{60} results 0.95 ± 0.09 in toluene. Obtained values fit very well with previously published results [40, 50] and prove that the method works well.

One measurement provides data for the calculation of both Φ_Δ and Φ_T. Triplet quantum yields Φ_T were computed according to the equation 3.15 with a result of 1.0 ± 0.1 for Thiazolyls (see table 4.1 and figure 4.11). The triplet energies of 850 nm were taken for both TPP and Thiazolyls (see section 4.8). The ratio Φ_Δ/Φ_T equals roughly 0.9 ± 0.1 for all samples in all solvents (see the table 4.1. It means that approximately 90% of triplets transfer energy to singlet oxygen (in agreement with [30]). We know that oxygen quenches more than 99% of triplets from the measurements of prolonged triplet lifetime in argon-saturated samples. Around 10% of triplets are quenched by oxygen but don't give rise to singlet oxygen. The high value of the Φ_Δ/Φ_T ratio means that energy transfer to singlet oxygen is definitely favoured compared to the generation of a superoxide radical. However, this statement cannot be generalized for more complex systems such as biological environment. The inaccuracy of the ratio Φ_Δ/Φ_T takes into account that the triplet energy needed for the calculation of Φ_T is not known precisely. Over-estimation of triplet energy would lead to under-estimated Φ_T and over-estimated ratio Φ_Δ/Φ_T. Under-estimation of the contractive structural volume change would lead to over-estimation of Φ_T and under-estimation of the ratio. It was explained before that structural volume changes are small for toluene. A possible under-estimation of structural change (resulting in an over-estimation of Φ_T) has to be considered in the case of THF and DMF (see section 3.8.1).

Triplet quantum yields in argon-saturated DMF were also determined by means of equation 3.15. Supposing the triplet energy of 850 nm for both TPP and Thiazolyls (see section 4.8) we get quantum yields $\Phi_T = 0.95 \pm 0.10$ for Thiazolyls and $\Phi_T = 0.65 \pm 0.10$ for TPP. The value for TPP corresponds to previously published results in the frame of experiment accuracy [29, 40] . In the case of argon-saturated samples, the sample signal can be fitted simply by the reference signal multiplied by a factor (only fast heat is present), which decreases inaccuracy of the result. If triplet quantum yields are known from other measurements, triplet energies can be calculated.

Finally, the triplet quantum yield Φ_T was alternatively calculated from 3.17. Results are shown in figure 4.12 for toluene. The parameter p was set to the value

of 0.9. It's obvious that the Φ_T values are more stable in the whole laser fluence region when compared to the calculation according to 3.15. The calculation method seems to be provide a bit more precise results due to the elimination of the effect of absorbance mismatch.

toluene				
	TPP	C_{60}	MonoThiazolyl	BiThiazolyl
Φ_Δ (lum., TPP ref.)	0.65	0.79	0.81	0.80
Φ_Δ (OA)	0.58	0.93	0.87	0.85
Φ_T (OA, eq. 3.15)	0.70	0.95	0.97	0.99
Φ_T (OA, eq. 3.17)	0.73	0.91	0.97	1.01
THF				
Φ_Δ (lum., TPP ref.)	0.65	−−	0.79	0.79
Φ_Δ (OA)	0.66	−−	0.96	0.93
Φ_T (OA, eq. 3.15)	0.80	−−	1.05	1.02
Φ_T (OA, eq. 3.17)	0.82	−−	1.04	1.01
DMF				
Φ_Δ (lum., TPP ref.)	0.65	−−	0.82	0.78
Φ_Δ (OA)	0.66	−−	1.03	1.00
Φ_T (OA, Ar, eq. 3.15)	0.65	−−	0.96	0.91

Table 4.1: Quantum yields by optoacoustic spectroscopy (OA) compared to luminescence measurements (lum.). The inaccuracy is estimated to be 10% in all the cases.

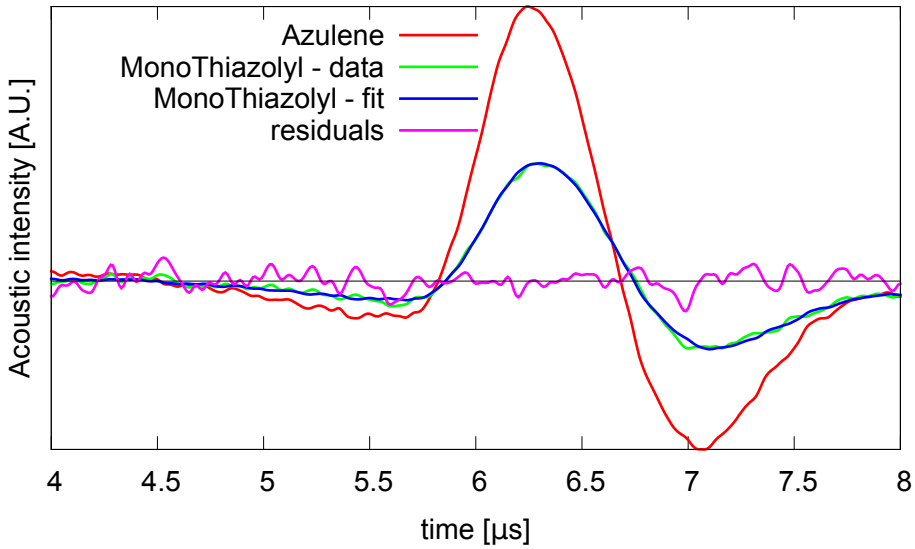

Figure 4.9: Typical optoacoustic signal of a sample compared to reference and fitted by the convolution 3.13. Residuals are shown.

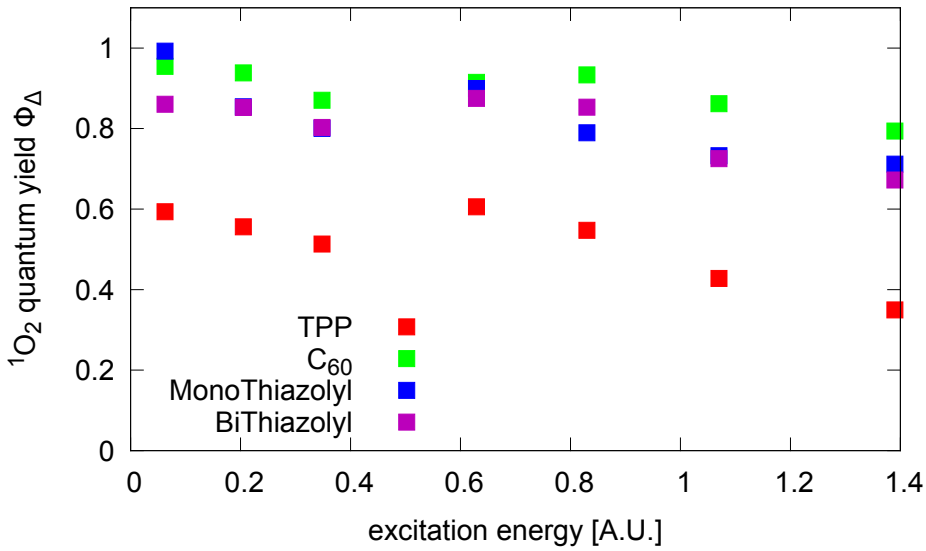

Figure 4.10: Quantum yield of singlet oxygen of TPP, Thiazolyls and C_{60} in toluene in dependence on laser fluence.

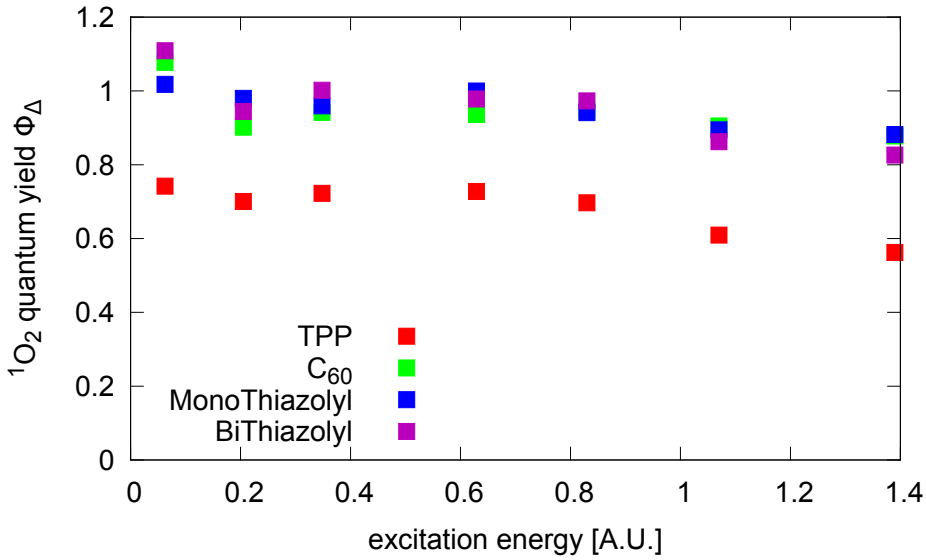

Figure 4.11: Triplet quantum yield of TPP, Thiazolyls and C_{60} in toluene in dependence on laser fluence.

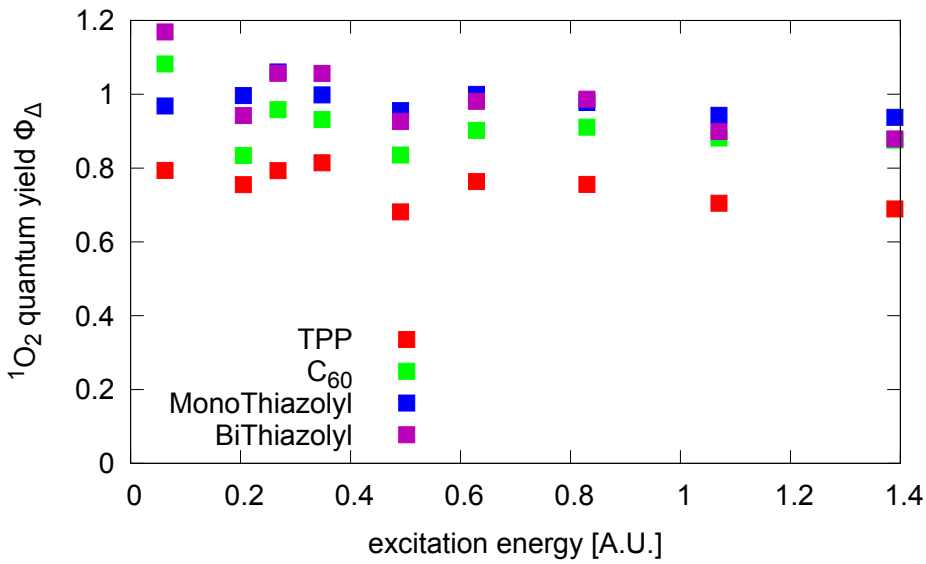

Figure 4.12: Triplet quantum yield of TPP, Thiazolyls and C_{60} in toluene in dependence on laser fluence based on q_1/q_2 ratio according to equation 3.17.

4.7 Delayed Fluorescence

The setup described in section 3.6 allowing time- and spectral-resolved measurements of luminescence was originally intended to be employed to detect the short-wavelength-portion of phosphorescence. A comparison of prompt fluorescence spectrum with the long-lived spectrum (overlapped DF and phosphorescence) would enable the separation of DF from phosphorescence. However, no such superimposed phosphorescence was observed probably due to very poor sensitivity of the detector at longer wavelengths. Nevertheless, a few interesting observations regarding DF were made.

Samples of TPP and MonoThiazolyl in nitrogen-saturated THF were prepared at absorbances of 0.5 at 420 nm which correspond to concentrations around 2 µM. Spectral shapes of DF and prompt fluorescence are almost identical (figure 4.13) after a subtraction of quadratic fit of broad-band background in the case of prompt fluorescence. The quantum yield of DF is more than ten-fold smaller for MonoThiazolyl than for TPP, which is in accordance with yields of prompt fluorescence. The quantum yield of DF was determined to be more than 100-fold smaller than quantum yields of prompt fluorescence for both TPP and MonoThiazolyl. It means that the repopulation of singlets is only a minor channel of triplet decay (supposing that the probability of radiative deactivation of repopulated excited singlets is not much smaller than the probability for prompt excited singlets). If so, model 3.7 doesn't have to be used either for triplet kinetics or for DF kinetics.

DF of TPP was measured with a 5 µs gate. Peak intensities of DF at 650 nm provide a time-series to be fitted. The peak intensity was obtained from a quadratic fit of the top of the main fluorescence band. Monoexponential fit provides a DF lifetime of 145 ± 10 µs which is approximately half of the triplet lifetime (295 ± 10 µs, see section 4.8 and figure 4.17). It suggests that triplet-triplet annihilation mechanism takes place. Data points are too sparse to be reasonably fitted by two exponentials with relatively close lifetimes according to 3.8. Such biexponential fit doesn't provide markedly better residuals and leads to great errors of parameters. DF of MonoThiazolyl is much weaker than that of TPP. A gate of 100 µs was used. The time-series of DF intensities fitted by

$$I_{\mathrm{DF}}(t) = A(e^{-t/\tau_{\mathrm{DF}}} - e^{-(t+\Delta t)/\tau_{\mathrm{DF}}}) \tag{4.1}$$

provides a DF lifetime of 32 ± 4 µs for Thiazolyls which is shorter than the triplet lifetime of 50 ± 10 µs. The Kinetics of DF is shown in figure 4.14 and turns out to be excellently monoexponential. Again, data points are too sparse to be reasonably fitted by two exponentials according to 3.8. Inaccuracies of lifetimes were calculated as a standard deviation of lifetimes obtained at a set of ten wavelengths around the fluorescence maximum.

4.8 Photosensitizer Phosphorescence

IR-luminescence spectra in nitrogen-saturated THF were detected by the setup for time- and spectrally-resolved luminescence described in section 3.7. Kinetics of IR-luminescence were measured for a range of wavelengths with a 16 nm step.

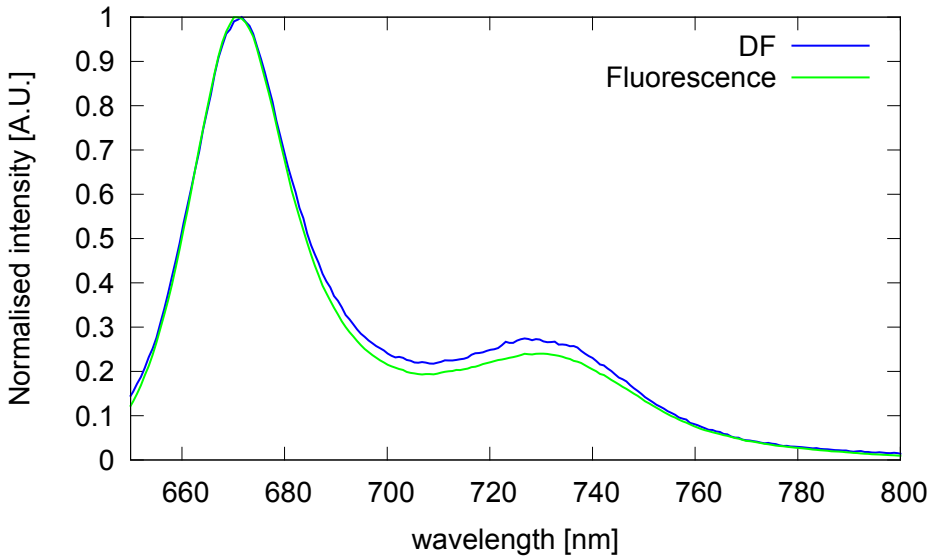

Figure 4.13: Prompt and delayed fluorescence of MonoThiazolyl (normalized) in nitrogen-saturated THF.

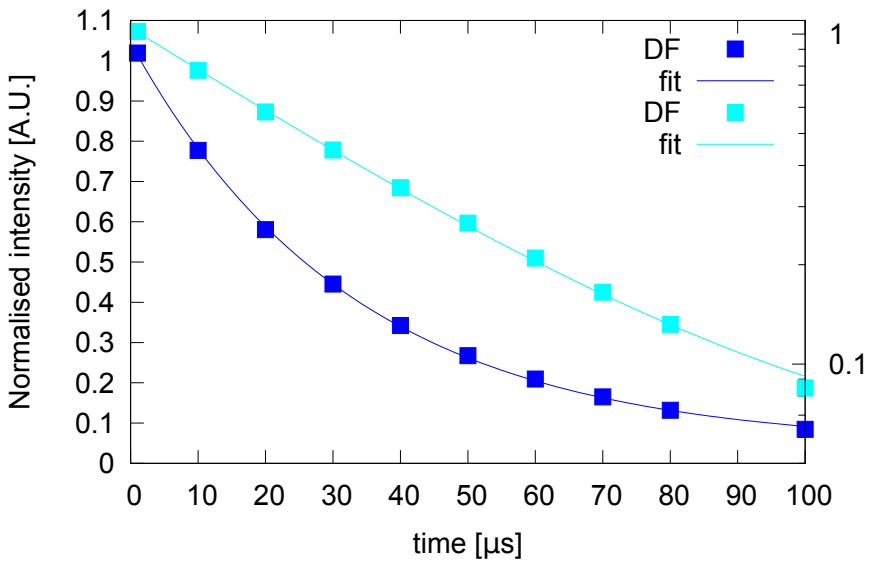

Figure 4.14: Delayed fluorescence of MonoThiazolyl in nitrogen-saturated THF fitted by 4.1. Logarithmic plot (brighter) is provided as well.

IR-luminescence kinetics were satisfactorily fitted by monoexponential function. Intensity was obtained as a fit value at zero time. Fast processes, such as prompt fluorescence and scattering, are cut off and do not interfere. IR-luminescence spectra are shown in figure 4.15.

As mentioned before, recorded IR-luminescence spectra can be a result of overlapped phosphorescence and delayed fluorescence. Lifetimes of DF are twice as short in the case of the triplet-triplet annihilation mechanism. Figure 4.16 shows lifetimes of IR-luminescence as a function of wavelength providing interesting information regarding the sparation of delayed fluorescence and phosphorescence. It's clearly visible that IR-luminescence lifetimes of Thiazolyls are $\sim$ 25 µs at shorter wavelengths and then the lifetime changes to $\sim$ 45 µs around wavelength of 850 nm. Lifetime of $\sim$ 45 µs perfectly matches the triplet lifetime obtained from T-S absorption measurements. It suggests that at wavelengths below 850 nm, delayed fluorescence induced by triplet-triplet annihilation mechanism takes place and is dominant. Phosphorescence dominates at wavelengths longer than 850 nm. Triplet energy of Thiazolyls of 850 $\pm$ 30 nm is thus obtained. Triplet energy of TPP was reported to be also around 850 nm [47]. TPP has higher quantum yield of delayed fluorescence (see section 4.7). Lifetimes of TPP IR-luminescence around 100 µs are pretty constant over wavelengths (data not shown). However, the triplet lifetime obtained from T-S absorption is 295 $\pm$ 10 µs. It clearly suggests that the IR-luminescence spectra obtained for TPP doesn't correspond to phosphorescence but rather to the tail of delayed fluorescence. The measurement of delayed fluorescence was described in section 4.7 giving a lifetime of 145 $\pm$ 10 µs. The DF lifetime is closer to IR-luminescence lifetime, but still do not match perfectly. The triplet lifetime, DF lifetime, and IR-luminescence lifetime measurements were all done with the same sample solution. The lifetime of TPP triplets and IR-luminescence were reproduced in frame of the experiment accuracy for newly prepared nitrogen-saturated control samples. (However, generally it may be difficult to prepare properly de-oxygenated samples and obtain reproducible triplet lifetimes in independent experiments.) The IR-luminescence lifetime didn't decrease during two consequential spectral-resolved measurements which lasted more than one hour in total. It means that a leakage of oxygen into the sample didn't take place. The inaccuracies of lifetimes were determined as standard deviations of a set of lifetimes obtained at different wavelengths. Figure 4.17 compares the kinetics of IR-luminescence, T-T absorption and delayed fluorescence.

The phosphorescence of Thiazolyls is directly observable at room temperature in deoxygenated samples. Triplet energy of 850 $\pm$ 30 nm is close to the value obtained for TPP at liquid nitrogen temperature [47]. The phosphorescence of Thiazolyls is remarkably extended to red. It's probable that the TPP spectrum at figure 4.15 is formed mainly by delayed fluorescence. Integral phosphorescence of Thiazolyls is then probably stronger than that of TPP. At least it was clearly proved that the phosphorescence of Thiazolyls is much stronger than that of TPP at wavelengths above 950 nm.

Decay lifetimes of phosphorescence of Thiazolyls (50$\pm$5 µs for MonoThiazolyl) perfectly match lifetimes obtained by flash-photolysis. Phosphorescence decays of MonoThiazolyl at various wavelengths recorded by the apparatus described in section 3.5 are shown in figure 4.18. Decays are perfectly monoexponential.

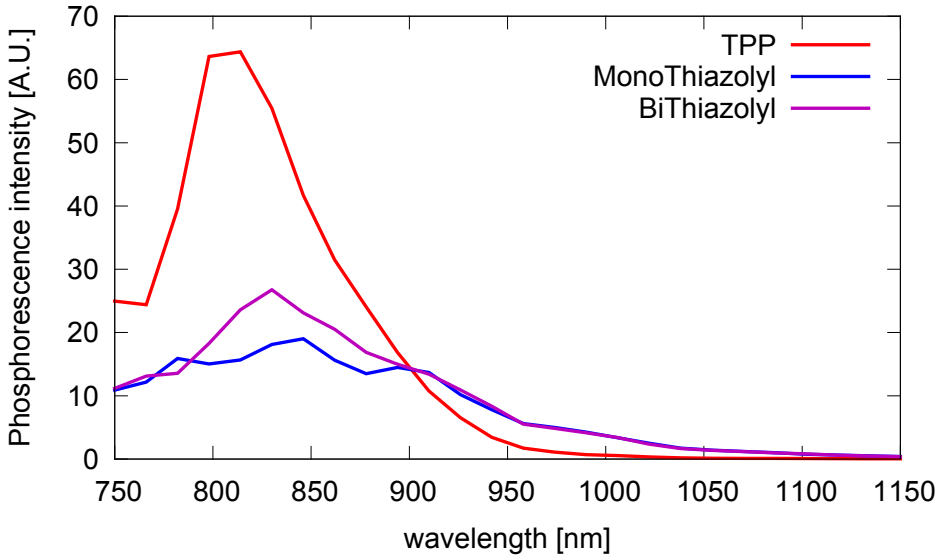

Figure 4.15: Phosphorescence overlapped by delayed fluorescence of TPP and Thiazolyls in THF based on time-resolved measurements.

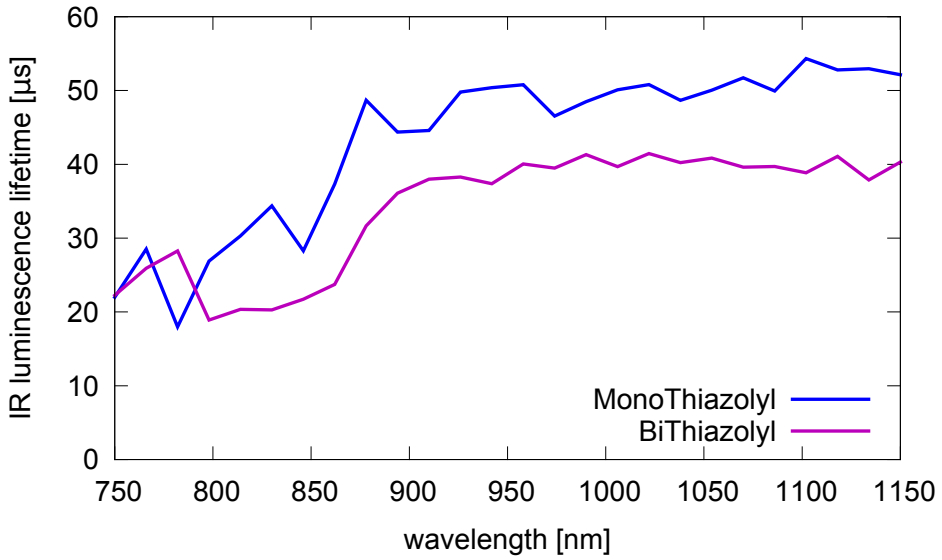

Figure 4.16: Lifetimes of Thiazolyls in THF as a function of wavelength.

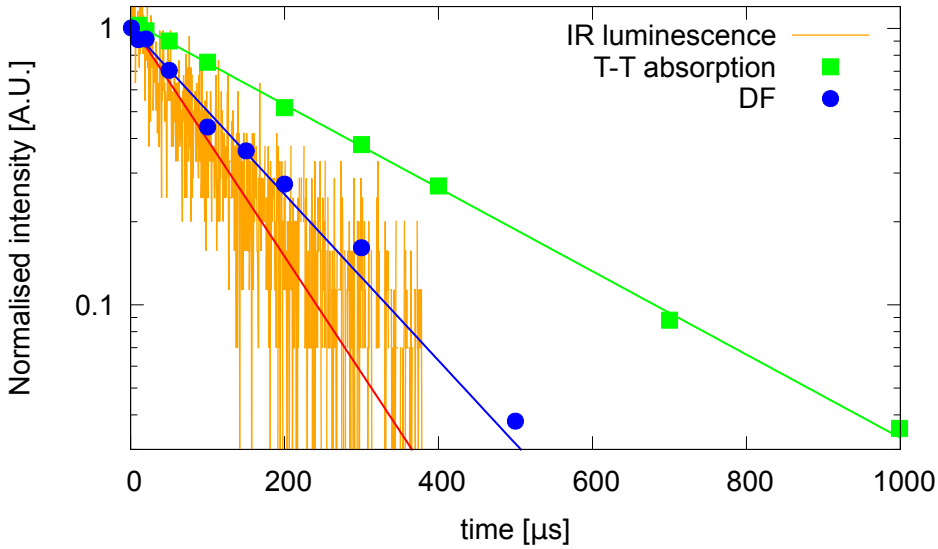

Figure 4.17: TPP: Comparison of kinetics from time-resolved IR-luminescence, triplet-triplet absorption and delayed fluorescence.

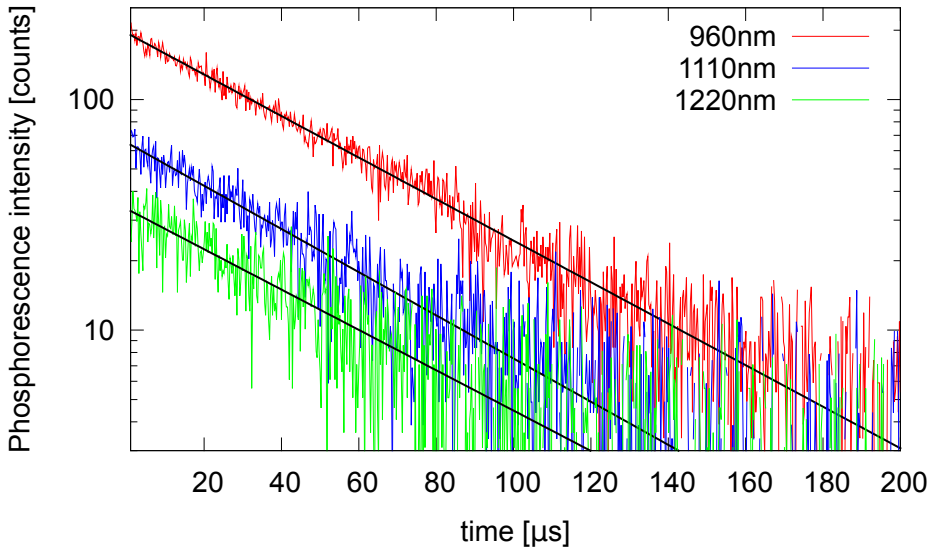

Figure 4.18: Phosphorescence decay of MonoThiazolyl at various wavelengths fitted by one exponential.

4.9 Microscopy

Dark current of CCD (charge accumulated even if CCD is in absolute dark) is a key parameter of CCD with respect to the ability to detect weak phosphorescence. Camera is cooled down to the minimal recommended temperature of $-55°C$ by Peltier cooler. Dark current significantly decreases as the temperature drops. Different pixels have different dark current rates and different sensitivities as well. There are some hot spots with extremely high dark current which are useless for signal detecting. Values of dark current accumulated during a given exposition time always have to be subtracted from signal image. Sensitivity of each pixel was determined from flatfield measurement. Qualitative map of the ratio (sensitivity)/(dark current) over the whole CCD is shown in figure 4.19. Such a map can be used to select the best part of the chip with the best signal-to-noise ratio. By moving the grating (at zero-order diffraction) the image can be shifted over the CCD. Exposition time of 1s proved to provide the best signal-to-noise ratio.

Spectrum of singlet oxygen emission from a solution was recorded as a proof-of-method experiment for the singlet-oxygen-microscope-setup (figure 4.20). Solution of 150 µM TPP in acetone in a quartz cuvette was placed in the sample-holder. The exposition time was set to 1s, slit-width to 30 nm and objective 4x was used. The illumination of CCD at the singlet oxygen emission band reached approximately 2% of the CCD range at its maximum. Thus, the ability of the system to detect singlet oxygen was proven.

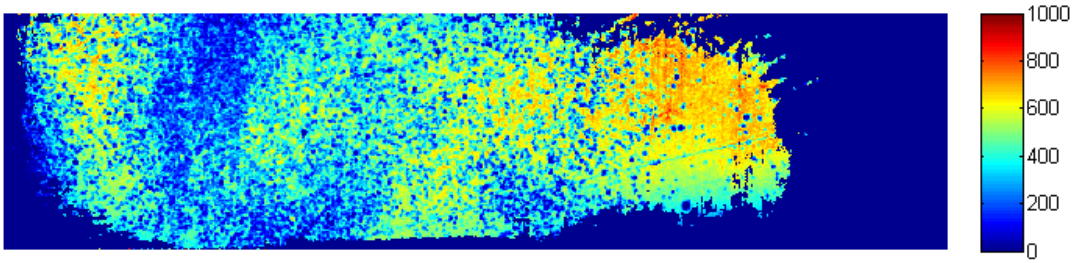

Figure 4.19: Map of the ratio (sensitivity)/(dark current) for each pixel over the whole CCD chip of MOSIR 950 camera. The pixels with the best ratio are marked by red color. Dark blue color indicates areas of pixels with sensitivities lower than one third of the best achieved sensitivities.

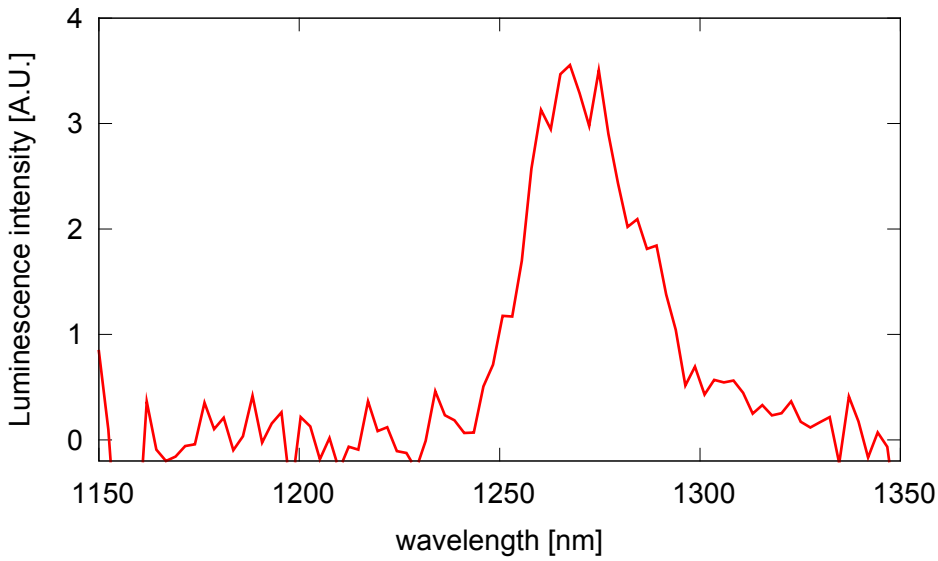

Figure 4.20: Spectrum of singlet oxygen phosphorescence observed by MOSIR 950 camera.

5 Conclusions

Thiazolyl-porphyrins are promising new photosensitizers with singlet oxygen quantum yields close to unity. Photophysical properties of Thiazolyls significantly differ from those of TPP. The introduction of four sulphur atoms results in an enhanced intersystem-crossing. A wide range of experimental techniques was employed in order to provide photophysical characterization of the compounds. The quantum yield of singlet oxygen production was determined to be 0.9 ± 0.1 for Thiazolyls in DMF, THF and toluene. The singlet oxygen quantum yield of TPP determined by optoacoustic spectroscopy was 0.65 ± 0.10 for all the solvents, which is in accordance with previously published results [40, 50]. The efficiency of energy transfer from PS triplet to singlet oxygen is around 90% for all the compounds. Quantum yield of fluorescence of Thiazolyls is close to 0.01 while 0.11 for TPP and fluorescence lifetimes for Thiazolyls are close to 1.5 ns while 10 ns for TPP. Non-radiative decay processes are thus remarkably enhanced. The phosphorescence of Thiazolyls is definitely remarkably stronger than that of TPP at wavelengths above 950 nm and probably stronger in the whole spectral region. The triplet energy of Thiazolyls was determined to be 850 ± 30 nm which is comparable to TPP. Triplet lifetimes of Thiazolyls in argon-saturated samples are much shorter than that of TPP (> 200 µs) resulting in values of 50 ± 10 µs both in DMF and THF. There is no difference in photostability between TPP and Thiazolyls. The high quantum yield of singlet oxygen promotes Thiazolyls as new standards and reference compounds. However, the worse solubility of Thiazolyls delimits the scope of possible applications.

An overview of several useful experimental techniques regarding photosensitizer photophysics was provided. Experimental and data-handling procedures for optoacoustic spectroscopy were improved leading to more reliable results of quantum yields. A unique experimental setup for direct microscopic observation of singlet oxygen luminescence directly in living cells is being developed and some promising results have been achieved.

The aims of the work were fulfilled. However, several new perspectives have emerged. Luminescence microscopy is an especially great challenge for further work.

toluene			
	TPP	Thiazolyl	BiThiazolyl
λ_{max}/nm	419(Soret)	427(Soret)	427(Soret)
	$515, 548, 591, 647$(Q)	$521, 557, 598, 664$(Q)	$521, 557, 598, 666$(Q)
λ_F/nm	$651, 717$	$668, 725$	$668, 725$
Φ_F	11%	(1.0 ± 0.2)%	(1.3 ± 0.2)%
τ_S /ns (air)	9.5 ± 0.2	1.4 ± 0.2	1.4 ± 0.2
τ_T /ns (air)	310 ± 10	250 ± 10	240 ± 10
Φ_Δ (lum.)	0.65(ref.)	0.8 ± 0.1	0.8 ± 0.1
Φ_Δ (OA)	0.65 ± 0.10	0.9 ± 0.1	0.9 ± 0.1
Φ_T (OA)	0.70 ± 0.10	0.95 ± 0.10	0.95 ± 0.10
Φ_Δ/Φ_T (OA)	0.9 ± 0.1	0.9 ± 0.1	0.9 ± 0.1
DMF			
λ_{max}/nm	417(Soret)	423(Soret)	423(Soret)
	$513, 547, 591, 647$(Q)	$520, 555, 597, 663$(Q)	$520, 555, 597, 663$(Q)
$\varepsilon/10^5 M^{-1}cm^{-1}$	4.6 ± 0.5	1.9 ± 0.2	2.6 ± 0.3
λ_F/nm	$651; 716$	$666; 723$	$666; 723$
Φ_F	$--$	(1.0 ± 0.2)%	(1.2 ± 0.2)%
τ_S /ns (air)	10.5 ± 0.2	1.5 ± 0.2	1.5 ± 0.2
τ_T /ns (air)	480 ± 10	400 ± 10	410 ± 10
τ_T / µs (Ar)	> 200	50 ± 10	50 ± 10
Φ_Δ (lum.)	0.65(ref.)	0.8 ± 0.1	0.8 ± 0.1
Φ_Δ (OA)	0.65 ± 0.05	0.9 ± 0.1	0.9 ± 0.1
Φ_T (OA, Ar)	0.65 ± 0.10	0.95 ± 0.10	0.95 ± 0.10
THF			
λ_{max}/nm	417(Soret)	423(Soret)	423(Soret)
	$513, 547, 591, 647$(Q)	$520, 555, 597, 663$(Q)	$520, 555, 597, 663$(Q)
λ_F/nm	$651; 716$	$666; 723$	$666; 723$
Φ_F	$--$	(1.0 ± 0.2)%	(1.2 ± 0.2)%
τ_S /ns (air)	10.0 ± 0.2	1.5 ± 0.2	1.5 ± 0.2
τ_T /ns (air)	320 ± 10	270 ± 10	280 ± 10
τ_T / µs (Ar)	> 295	50 ± 10	50 ± 10
Φ_Δ (lum.)	0.65(ref.)	0.8 ± 0.1	0.8 ± 0.1
Φ_Δ (OA)	0.65 ± 0.05	0.9 ± 0.1	0.9 ± 0.1
Φ_T (OA)	0.75 ± 0.10	1.0 ± 0.1	1.0 ± 0.1
Φ_Δ/Φ_T (OA)	0.9 ± 0.1	0.9 ± 0.1	0.9 ± 0.1
E_T/nm	$--$	850 ± 30	850 ± 30

Table 5.1: Photophysical properties of TPP and Thiazolyls in toluene. Legend: λ_{max}: absorption maxima, λ_F: fluorescence maxima, Φ_F: fluorescence quantum yield, τ_S: fluorescence (singlet) lifetime, τ_T: PS triplet lifetime, Φ_Δ: singlet oxygen quantum yield, Φ_T: PS triplet quantum yield, E_T: energy of PS triplet, OA: optoacoustic experiment, lum.: $^1O_2$ phosphorescence experiment, air: air-saturated sample, Ar: argon-saturated sample.

Bibliography

[1] ALI, H. – LIER, J. E. *Porphyrins and Phthalocyanines as Photosensitizers and Radiosensitizers, in Handbook of Porphyrin Science*. volume 4. : World Scientific Publishing, 1999. ISBN 0123932009.

[2] ALLISON, R. R. – SIBATA, C. H. Oncologic photodynamic therapy photosensitizers: A clinical review. *Photodiagnosis and Photodynamic Therapy*. 2010, 7, number 2, p. 61 – 75. doi: DOI: 10.1016/j.pdpdt.2010.02.001.

[3] AWAN, M. – TARIN, S. Review of photodynamic therapy. *The Surgeon*. 2006, 4, number 4, p. 231 – 236. doi: DOI: 10.1016/S1479-666X(06)80065-X.

[4] AZENHA, E. G. et al. Heavy-atom effects on metalloporphyrins and polyhalogenated porphyrins. *Chemical Physics*. 2002, 280, number 1-2, p. 177 – 190. doi: 10.1016/S0301-0104(02)00485-8.

[5] BAIER, J. et al. Theoretical and experimental analysis of the luminescence signal of singlet oxygen for different photosensitizers. *Journal of Photochemistry and Photobiology B: Biology*. 2007, 87, number 3, p. 163–173.

[6] BANSAL, A. et al. Absorption and emission spectroscopic characterization of platinum-octaethyl-porphyrin (PtOEP). *Chemical Physics*. 2006, 330, number 1-2, p. 118 – 129. doi: 10.1016/j.chemphys.2006.08.002.

[7] BECHET, D. et al. Nanoparticles as vehicles for delivery of photodynamic therapy agents. *Trends in Biotechnology*. 2008, 26, number 11, p. 612 – 621. doi: 10.1016/j.tibtech.2008.07.007.

[8] BECKER, W. *Advanced Time-Correlated Single Photon Counting Techniques*. volume 1. : Springer, 2005. ISBN 3-540-26047-1.

[9] BRASLAVSKY, S. – HEIBEL, G. Time-resolved photothermal and photoacoustic methods applied to photoinduced processes in solution. *Chemical Reviews*. 1992, 92, number 6, p. 1381–1410.

[10] BRASLAVSKY, S. E. et al. Photophysical properties of porphycene derivatives (18 [pi] porphyrinoids). *Journal of Photochemistry and Photobiology B: Biology*. 1997, 40, number 3, p. 191 – 198. doi: 10.1016/S1011-1344(97)00075-4.

[11] BUYTAERT, E. – DEWAELE, M. – AGOSTINIS, P. Molecular effectors of multiple cell death pathways initiated by photodynamic therapy. *Biochimica et Biophysica Acta (BBA) - Reviews on Cancer*. 2007, 1776, number 1, p. 86 – 107. doi: DOI: 10.1016/j.bbcan.2007.07.001.

[12] CASTANO, A. – DEMIDOVA, T. – HAMBLIN, M. Mechanisms in photodynamic therapy: part one —— photosensitizers, photochemistry and cellular localization. *Photodiagnosis and Photodynamic Therapy*. 2004, 1, p. 279–293.

[13] CASTANO, A. – DEMIDOVA, T. – HAMBLIN, M. Mechanisms in photodynamic therapy: part two——cellular signaling, cell metabolism and modes of cell death. *Photodiagnosis and Photodynamic Therapy*. 2005, 2, p. 1–23.

[14] CASTANO, A. – DEMIDOVA, T. – HAMBLIN, M. Mechanisms in photodynamic therapy: Part three——Photosensitizer pharmacokinetics, biodistribution, tumor localization and modes of tumor destruction. *Photodiagnosis and Photodynamic Therapy*. 2005, 2, p. 91–106.

[15] CHATTERJEE, D. K. – FONG, L. S. – ZHANG, Y. Nanoparticles in photodynamic therapy: An emerging paradigm. *Advanced Drug Delivery Reviews*. 2008, 60, number 15, p. 1627 – 1637. doi: 10.1016/j.addr.2008.08.003. 2008 Editors' Collection.

[16] CLENNAN, E. – PACE, A. Advances in singlet oxygen chemistry. *Tetrahedron*. 2005, 61, number 28, p. 6665–6691.

[17] DAI, T. – HUANG, Y.-Y. – HAMBLIN, M. R. Photodynamic therapy for localized infections–State of the art. *Photodiagnosis and Photodynamic Therapy*. 2009, 6, number 3-4, p. 170 – 188. doi: DOI: 10.1016/j.pdpdt.2009.10.008.

[18] DAVYDOV, A. *Kvantová mechanika*. volume 1. : SPN, Praha, 1978.

[19] DĚDIC, R. et al. Phosphorescence of singlet oxygen and meso-tetra(4-sulfonatophenyl)porphin: time and spectral resolved study. *Journal of Molecular Structure*. 2003, 651-653, p. 301 – 304. doi: 10.1016/S0022-2860(02)00645-2. Molecular Spectroscopy and Molecular Structure 2002. Proceedings of the XXVIth European Congress on Molecular Spectroscopy, Villeneuve d'Ascq, France, September 1-6, 2002.

[20] DOUGHERTY, T. J. – POTTER, W. R. Of what value is a highly absorbing photosensitizer in PDT? *Journal of Photochemistry and Photobiology B: Biology*. 1991, 8, number 2, p. 223 – 223. doi: 10.1016/1011-1344(91)80063-N.

[21] EGOROV, G. – KOLKER, A. The Thermal Properties of Water-N,N-Dimethylformamide Solutions at 278-323.15 K and 0.1-100 MPa. *Russian Journal Of Physical Chemistry A*. 2008, 82, number 12, p. 2058–2064.

[22] FIGGE, F. – WEILAND, G. – LO, L. M. Cancer detection and therapy; affinity of neoplastic, embryonic, and traumatized tissues for porphyrins and metalloporphyrins. *Proceedings of the Society for Experimental Biology and Medicine*. 1948, 68, number 3, p. 640–641.

[23] GARCÍA-DÍAZ, M. et al. Do folate-receptor targeted liposomal photosensitizers enhance photodynamic therapy selectivity? *Biochimica et Biophysica Acta (BBA) - Biomembranes*. 2011, 1808, number 4, p. 1063 – 1071. doi: 10.1016/j.bbamem.2010.12.014.

[24] GENSCH, T. – VIAPPIANI, C. Time-resolved photothermal methods: accessing time-resolved thermodynamics of photoinduced processes in chemistry and biology. *Photochemical & Photobiological Sciences*. 2003, 2, number 7, p. 699–721.

[25] GENSCH, T. – VIAPPIANI, C. – BRASLAVSKY, S. Structural volume changes upon photoexcitation of porphyrins: Role of the nitrogen - Water interactions. *Journal of the American Chemical Society*. 1999, 121, number 45, p. 10573–10582.

[26] GENSCH, T. – VIAPPIANI, C. – BRASLAVSKY, S. *Laser Induced Optoacoustic Spectroscopy, in Encyclopedia of Spectroscopy and Spectrometry*. volume 1. : Academic Press, 2000. ISBN 0-12-226680-3.

[27] GILBERT, D. L. – COLTON, C. A. *Reactive Oxygen Species in Biological Systems*. volume 1. : Kluwer Academic / Plenum Publishers, New York, 1999. ISBN 0-306-45756-3.

[28] GORMAN, A. et al. In vitro demonstration of the heavy-atom effect for photodynamic therapy Record contains structures. *Journal of the American Chemical Society*. 2004, 126, number 34, p. 10619–10631.

[29] HA, J.-H. et al. Effect of core atom modification on photophysical properties and singlet oxygen generation efficiencies: tetraphenylporphyrin analogues core-modified by oxygen and/or sulfur. *Chemical Physics Letters*. 2001, 349, number 3-4, p. 271 – 278. doi: 10.1016/S0009-2614(01)01231-3.

[30] HA, J. et al. Photophysical Efficiency Factors of Singlet Oxygen Generation from Core-modified Trithiasapphyrin Derivatives. *Bulletin of the Korean Chemical Society*. 2002, 23, number 2, p. 281–285.

[31] HAMBLIN, M. R. – NEWMAN, E. L. New trends in photobiology: On the mechanism of the tumour-localising effect in photodynamic therapy. *Journal of Photochemistry and Photobiology B: Biology*. 1994, 23, number 1, p. 3 – 8. doi: 10.1016/S1011-1344(94)80018-9.

[32] Intevac Photonics. MOSIR 950 Infrared Camera datasheet.

[33] ISHIZUKA, M. et al. Novel development of 5-aminolevulinic acid (ALA) in cancer diagnoses and therapy. *International Immunopharmacology*. 2011, 11, number 3, p. 358 – 365. doi: 10.1016/j.intimp.2010.11.029. Immunopharmacology of Synthetic Natural Products.

[34] JORI, G. – REDDI, E. The role of lipoproteins in the delivery of tumour-targeting photosensitizers. *International Journal of Biochemistry & Cell Biology*. 1993, 25, number 10, p. 1369—1375. doi: 10.1016/0020-711X(93)90684-7.

[35] LAKOWICZ, J. *Principles of fluorescence spectroscopy*. volume 1. : Plenum Press, New York, 1983. ISBN 0-306-41285-3.

[36] LIDE, D. R. *CRC Handbook of Chemistry and Physics, 87th ed.* volume 1. : CRC Press/Taylor and Francis Group, 2006. ISBN 0-8493-0487-3.

[37] LU, Y. – LOW, P. S. Folate-mediated delivery of macromolecular anticancer therapeutic agents. *Advanced Drug Delivery Reviews*. 2002, 54, number 5, p. 675 – 693. doi: 10.1016/S0169-409X(02)00042-X. Polymer Conjugates for Cancer Therapy.

[38] MARTÍ, C. et al. Aromatic ketones as standards for singlet molecular oxygen O2(1[Delta]g) photosensitization. Time-resolved photoacoustic and near-IR emission studies,. *Journal of Photochemistry and Photobiology A: Chemistry*. 1996, 97, number 1-2, p. 11 – 18. doi: 10.1016/1010-6030(96)04321-3.

[39] OGILBY, P. Singlet oxygen: there is still something new under the sun, and it is better than ever. *Photochemical & Photobiological Sciences*. 2010, 9, number 12, p. 1543–1560.

[40] REDMOND, R. – GAMLIN, J. A compilation of singlet oxygen yields from biologically relevant molecules. *Photochemistry and photobiology*. 1999, 70, number 4, p. 391–475.

[41] SCHMIDT, R. et al. Phenalenone, a universal reference compound for the determination of quantum yields of singlet oxygen O2(1[Delta]g) sensitization. *Journal of Photochemistry and Photobiology A: Chemistry*. 1994, 79, number 1-2, p. 11 – 17. doi: 10.1016/1010-6030(93)03746-4.

[42] SCHWEITZER, C. – SCHMIDT, R. Physical Mechanisms of Generation and Deactivation of Singlet Oxygen. *Chemical Reviews*. 2003, 103, number 5, p. 1685–1757.

[43] SEYBOLD, P. G. – GOUTERMAN, M. Porphyrins : XIII: Fluorescence spectra and quantum yields. *Journal of Molecular Spectroscopy*. 1969, 31, number 1-13, p. 1 – 13. doi: 10.1016/0022-2852(69)90335-X.

[44] SNYDER, J. et al. Optical detection of singlet oxygen from single cells. *Physical Chemistry Chemical Physics*. 2006, 8, number 37, p. 4280–4293.

[45] SZURKO, A. et al. Spectroscopic and biological studies of a novel synthetic chlorin derivative with prospects for use in PDT. *Bioorganic & Medicinal Chemistry*. 2009, 17, number 24, p. 8197 – 8205. doi: 10.1016/j.bmc.2009.10.029.

[46] TERAZIMA, M. – AZUMI, T. A time-resolved photoacoustic method with pulsed laser excitation in the condensed phase : the relation between signal intensity and decay-rate constant. *Bulletin Of The Chemical Society Of Japan*. 1990, 63, number 3, p. 741–745.

[47] VÖLCKER, A. et al. Near-infrared phosphorescence emission of compounds with low-lying triplet states. *Chemical Physics Letters*. 1989, 159, number 1, p. 103 – 108. doi: 10.1016/S0009-2614(89)87462-7.

[48] WEBSTER, S. – PECELI, D. – AL., H. H. Near-Unity Quantum Yields for Intersystem Crossing and Singlet Oxygen Generation in Polymethine-like Molecules: Design and Experimental Realization. *Journal of Physical Chemistry Letters*. 2010, 1, number 15, p. 2354–2360.

[49] Wikipedia. Molecular orbitals of singlet oxygen [online]. http://en.wikipedia.org/wiki/Singlet_oxygen, Uploaded 11.5.2007, viewed 1.6.2009.

[50] WILKINSON, F. – HELMAN, W. – ROSS, A. Quantum yields for the photosensitized formation of the lowest electronically excited singlet state of molecular oxygen in solution. *Journal of Physical and Chemical Reference Data*. 1993, 22, number 1, p. 113–262.

[51] YUAN, F. et al. Microvascular permeability of albumin, vascular surface area, and vascular volume measured in human adenocarcinoma LS174T using dorsal chamber in SCID mice. *Microvascular Research*. 1993, 45, number 3, p. 269–289.

[52] ZHAO, B. et al. Enhanced photodynamic efficacy towards melanoma cells by encapsulation of Pc4 in silica nanoparticles. *Toxicology and Applied Pharmacology*. 2009, 241, number 2, p. 163 – 172. doi: 10.1016/j.taap.2009.08.010.

List of Abbreviations

$^1O_2$	.....	singlet oxygen
Δ	.....	refers to lowest form of singlet oxygen (used especially in indices)
PS	.....	Photosensitizer
T_1	.....	triplet state of photosensitizer
τ_T	.....	lifetime of photosensitizer triplet
τ_Δ	.....	singlet oxygen lifetime
τ_S	.....	lifetime of first excited singlet of photosensitizer (fluorescence lifetime)
Φ_Δ	.....	quantum yield of singlet oxygen
Φ_T	.....	quantum yield of photosensitizer triplet
Φ_F	.....	quantum yield of fluorescence
TPP	.....	tetra-phenyl-porphyrin
THF	.....	tetra-hydro-furan
DMF	.....	di-methyl-formamide
PDT	.....	Photodynamic therapy
DF	.....	Delayed fluorescence
CCD	.....	Coupled charge device
IRF	.....	Instrument response function
PMT	.....	Photomultiplier

Attachment: Octave code

Crucial parts of Octave source code for processing data from optoacoustic spectroscopy (simplified).

```
    %determination of fit-range
idxs = find(x>=xmin & x<=xmax);
    %initial values of fit parameters
p0 = [0.5 0.5 0 0]
    %The dependence y(x) is fitted in given range
    %by Levenberg-Marquardt least squares method.
    %Output variable p contains values of fit-parameters.
[yfit,p] = leasqr(x(idxs),y(idxs),p0,@fitfun);

    %my_conv(u,v) calculates convolution of two vectors u,v.
    %The result is a vector of the same length.
function retval = my_conv(u,v)
        n = length(u);
        A = zeros(n);
        v = fliplr(v);
        for ii = 1:n
        A(ii,1:ii) = v(n-ii+1:n);
        end
        retval = A*u';
end

   %Fitfun(x,p) is called by leasqr function.
   %It returns values of fit-function for given parameters.
   %m_opt is a global structure containing
   %additional values which have to be passed to fitfun.
function retval = fitfun(x,p)
    global m_opt
    R = m_opt.yref;   %IRF is loaded into variable R
    xc = x - x(1);
    if ((m_opt.tau>0) & (m_opt.flagshift))
            %decay function of triplets (slow heat)
        g1 = exp(-xc/m_opt.tauT);
        g1 = p(1)*g1/sum(g1);
            %decay function of excited singlets (fast heat)
        g2 = exp(-xc/m_opt.tauF);
        g2 = p(2)*g2/sum(g2);
            %time-shift of IRF
        yr = interp1(1:length(R),R,x-p(4));
            %calculation of IRF and decay functions computed
        retval = my_conv(g1',yr')+my_conv(g2',yr')+p(3);
        retval = retval(1:length(x));
    end
end
```